RADIATIVE COOLING WITH THERMOELECTRIC FOR POWER GENERATION

NICHOLAS TANG KAH FAI

UNIVERSITI TUNKU ABDUL RAHMAN

RADIATIVE COOLING WITH THERMOELECTRIC FOR POWER GENERATION

NICHOLAS TANG KAH FAI

A project report submitted in partial fulfilment of the requirements for the award of Bachelor of Engineering (Honours) Mechanical Engineering

**Lee Kong Chian Faculty of Engineering and Science
Universiti Tunku Abdul Rahman**

September 2022

DECLARATION

I hereby declare that this project report is based on my original work except for citations and quotations which have been duly acknowledged. I also declare that it has not been previously and concurrently submitted for any other degree or award at UTAR or other institutions.

Signature :

Name : Nicholas Tang Kah Fai

ID No. : 1806133

Date : 11/09/2022

APPROVAL FOR SUBMISSION

I certify that this project report entitled "**RADIATIVE COOLING WITH THERMOELECTRIC FOR POWER GENERATION**" was prepared by **NICHOLAS TANG KAH FAI** has met the required standard for submission in partial fulfilment of the requirements for the award of Bachelor of Engineering (Honours) Mechanical Engineering at Universiti Tunku Abdul Rahman.

Approved by,

Signature   :   *Jun HK*

Supervisor   :   Dr. Jun Hieng Kiat

Date   :   12/09/2022

Signature   :

Co-Supervisor   :

Date   :

ACKNOWLEDGEMENTS

Firstly, I would like to express my gratitude and appreciation towards Dr Jun Hieng Kiat who is my supervisor for this final year project. A million thanks to his excellent guidance as well as his continuous support. His patience and advice had been a major factor leading to the completion of this research. Moreover, I would also like to thank my moderator for this project that is Dr Yew Ming Chian. He stated out my mistake and gave guidance on how to improve them both in my report and presentation. I would also like to thank the lab officers for their help in terms of preparing the equipment and apparatus needed for the research even though each of them is having a busy schedule. In addition, I would like to express my eternal gratitude towards my family as they had given endless support whether physically or mentally as well as financially. Not to mention that I would like to take this opportunity to thank my friends and course mates who had helped and encouraged me before. Lastly, this final year project had been completed on time.

ABSTRACT

Electricity is one of the many energies that are needed by human beings in this 21st century. Thermoelectric generators (TEG) are solid-state semiconductor devices that utilize the Seebeck effect which is able to produce electricity by harvesting energy from the heat flux. Temperature difference across the semiconductors lead to the production of power. Radiative cooling can be implemented together with thermoelectric generators for power generation as it is a passive cooling method that requires no external energy source. This project aims to develop a simple prototype model of radiative cooling-thermoelectric generator. This project can contribute to the studies of methods to generate power without harming the environment radiative cooling with thermoelectric for power generation can be used for all day application and radiative cooling requires no external energy source. Furthermore, to understand different materials used for radiative cooling and their performance. Silicon dioxide (SiO_2) and titanium dioxide (TiO_2) was chosen as the materials for the radiative cooling coating. Both SiO_2 and TiO_2 were characterized using scanning electron microscope with energy dispersive X-ray (SEM) and X-ray diffraction (XRD). Three prototypes of the different radiative coating were developed in this project. Prototype A which had single-layer SiO_2 coating, Prototype B which had single-layer TiO_2 coating and Prototype C which had double-layer radiative coating with SiO_2 coating as the bottom layer and TiO_2 coating as the top layer. A few parameters were studied throughout this project, and they are the temperature of the hot and cold sides of the TEG modules, the voltage generated by the prototypes and power generated. Data was captured for 24 hours for each prototype. From the experimental results, prototype C which is the prototype with a double-layer radiative cooling coating showed to have performed better than the other two prototypes. Prototype C managed to generate a peak voltage of 96.5 mV and the average voltage generated was 29.2 mV. Furthermore, the average temperature difference for prototype C was 1.4 °C and the average power generated was 0.655 mW. Prototype C had a 267.98% increase in terms of performance for average power generation and a 93.74% increase in terms of performance for average voltage generated as compared to prototype A.

TABLE OF CONTENTS

CHAPTER

LIST OF TABLES

LIST OF FIGURES

LIST OF SYMBOLS / ABBREVIATIONS

μm	Micrometer
°C	Degree Celsius
Al	Aluminium
BE	Broadband Emitter
CO_2	Carbon Dioxide
DT	Temperature difference
EDX	Energy Dispersive X-ray
FT-IT	Fourier-transform infrared
HFC	Hydrofluorocarbon
HfO_2	Hafnium Oxide
IR	Infrared Radiation
K	Kelvin
LWIR	Long-wave infrared
MIR	Mid-IR
mV	Millivolt
mW	Milliwatt
nm	Nanometer
O_2	Oxygen
O_3	Ozone
PDMS	Polydimethylsiloxane
PE	Polyethylene
PMMA	Polymethyl Methacrylate
P_{net}	Net Cooling Power
P_{nonrad}	Non-radiative heat transfer between surrounding and surface of the cooling material
P_{rad}	Thermal radiation power from surface
P_{solar}	Atmospheric radiation power absorbed on the surface
PVA	Polyvinyl alcohol
PVC	Polyvinyl Chloride
PVDF	Polyvinylidene Fluoride
PW	Precipitable Water
SE	Selective Emitter

SEM	Scanning Electron Microscope
SiO	Silicon Monoxide
SiO_2	Silicon Dioxide
TE	Thermoelectric
TEDLAR	Polyvinyl-fluoride polymer film
TEG	Thermoelectric Generator
TiO_2	Titanium Dioxide
TPX	Polymethyl Pentene
W	Watt
W/m^2	Watt per metre square
XRD	X-ray Diffraction

LIST OF APPENDICES

CHAPTER 1

INTRODUCTION

1.1   General Introduction

Electricity is one of the many energies that are needed by human beings in this 21st century. However, there are people around the world that still lack access to electricity. In order to combat this issue, electricity can be generated by harvesting energy from the environment. Energy could be harvested from various sources such as light which is the solar energy harvesting technique. But due to the fact that method could only work during the day and where there is direct sunlight. Some places on Earth have a rather limited amount of sunlight per day thus having limited access to solar energy for months. Leading from that, it is crucial to implement another method to passively generate power during the day and nighttime.

Thermoelectric generators (TEG) are solid-state semiconductor devices that utilize the Seebeck effect which is able to produce electricity by harvesting energy from the heat flux (Liu et al., 2021). Thus, by using TEG all-day power generation is achievable. Inside a TEG consist of thermocouples which are made of 1 p-type and 1 n-type semiconductor. Both semiconductors are connected in series by a metal strip. As mentioned earlier, the TEG utilizes the Seebeck effect which is defined to convert the energy of heat into voltage potential. For the Seebeck effect to occur, the movement of charge carriers inside the semiconductors needs to be present. In simple terms, diffusion of charge carriers occurs from the hot side to the cold side. Thus, leading to an accumulation of charge carriers at the opposite end. Which in the end leads to a generation of voltage potential which is directly proportional to the temperature difference across the semiconductor.

Power can be generated during the day and night by using the benefits of radiative cooling which is a passive cooling method that requires no external energy source. This is done by placing a thermal emitter on top of the TEG, whereby the thermal emitter emits heat radiatively into space. Radiative cooling is a passive cooling process that involves radiating thermal radiation to outer

space to cool down a surface or body (Bin et al., n.d.). A radiative cooling system emits thermal radiation from the surface of Earth to outer space through an atmospheric long-wave infrared (LWIR) transmission window (8-13 µm).

1.2   Importance of Study

The application of radiative cooling with thermoelectric for power generation can be used to combat issues regarding energy supply as thermoelectric generators can be used as passive electricity generator and radiative cooling requires no external energy source. Some rural areas located around the world have limited supply of electricity and they can benefit from power generated by using radiative cooling with thermoelectric. Furthermore, by using radiative cooling with thermoelectric for power generation, the impact of global warming and greenhouse gas emission can be reduced, which is a more environment-friendly option. On the other hand, wasted heat energy can be recycled as well to help the power generation by thermoelectric.

1.3   Problem Statement

Electricity is very much needed in the daily life of human beings in the 21st century. However, there are some areas in the world where access to electricity is limited. The global energy supply is decreasing due to the rapid growth of the world population and industrial development. This causes pollution of the environment or in other words environmental degradation. The questions are whether there is a sustainable way to produce energy without harming the environment. By utilizing radiative cooling with thermoelectric for power generation, no external energy source is needed hence leading to reduction in environmental pollution. Since the efficiency of the radiative cooling system depends on the material and structures of the radiative cooler, different materials and methods have been proposed. Radiative cooling occurs when thermal radiation is emitted through an atmospheric window (8-13 µm). However, different materials have different thermal emittances and solar reflectance. The problem statement is what material is the most suitable for radiative cooling with thermoelectric to generate the most power and highest efficiency.

1.4   Aims and Objectives

The aim of the research is to investigate different materials used for radiative cooling and apply them with thermoelectric for power generation. The objectives of the project are:

- To develop a simple prototype model of radiative cooling-thermoelectric generator
- To investigate the effect of different materials and structures on radiative cooling
- To evaluate the performance of the radiative cooling-thermoelectric generator

1.5   Scope and limitation of study

This project mainly is to build a prototype that utilizes radiative cooling with thermoelectric for power generation. In order to do this, radiative cooling material is needed to be prepared. However, in Malaysia whereby the weather is hot and humid, and will often rain. The weather is unpredictable. Hence, the different weather conditions will have a different effect on the project as the project is needed to be carried out outdoors.

1.6   Contribution of Study

The overview of the project is to address the issue of environmental pollution caused when generating power. Most researchers are making efforts to find ways and improvements to generate power without causing harm to the environment and reducing the effect of global warming. Most importantly the method for power generation has to be sustainable and affordable. Hence, this project can contribute to the studies of methods to generate power without harming the environment as radiative cooling with thermoelectric for power generation can be used for all day application and radiative cooling requires no external energy source. Furthermore, to understand different materials used for radiative cooling and their performance.

1.7 Outline of Report

In this report, it consists of five chapters in total. Where this report starts with the introduction section, moving on to the literature review and followed by the methodology, results and discussion and lastly the conclusion and recommendations.

Chapter 1 displays the general introduction of radiative cooling and thermoelectric which presents the fundamentals of thermoelectric generators and radiative cooling. This chapter also includes the importance of study, objectives of the project, problem statement, scope and limitation of study and the contribution of study.

Chapter 2 is the literature review whereby it provides a detailed discussion of radiative cooling and thermoelectric. This chapter also includes factors that affect radiative cooling efficiency as well as the different materials used for radiative cooling and their properties. Furthermore, this chapter also includes discussion that involves radiative cooling with thermoelectric for power generation.

Chapter 3 is the methodology section of the project. This chapter provides a complete and detailed overview of the choices of materials and the complete experimental steps to study different materials used for radiative cooling with thermoelectric for power generation.

Chapter 4 presents the results and discussion of the project. This chapter includes all findings from the experiment and includes discussion based on the data gathered from the experiment.

Chapter 5 is the conclusion and recommendation part of the project. This chapter includes summary of the entire project and states some recommendations that can be used for improvement for this research project.

CHAPTER 2

LITERATURE REVIEW

2.1   Radiative Cooling

2.1.1   Fundamentals of Radiative Cooling

Radiative cooling occurs by emitting thermal radiation through an atmospheric window into outer space which has a temperature reading of around 3 K. This is a very transparent window in the infrared wavelength range from 8 to 13 µm (Hossain and Gu., 2016). Within that infrared wavelength range, the Earth's atmosphere has weak radiative emission, however, outside of that range, the Earth's atmosphere has high radiative emission. Outer space now acts as a large thermal reservoir whereby thermal radiation is emitted through the Earth's atmosphere. Figure 2.1 shows the Earth's surface and the arrows indicate energy flows. A device is needed for radiative cooling which is a thermal emitter. There are several thermal emitters, but for example, there is a broadband emitter (BE) and a selective emitter (SE). A broadband emitter has a strong emissivity in the whole mid-IR (MIR) spectrum (Ishii et al., 2020). On the other hand, a selective emitter is more effective in terms of emissivity as it only has a strong emissivity in the atmospheric window which is between 8 µm to 13 µm wavelength.
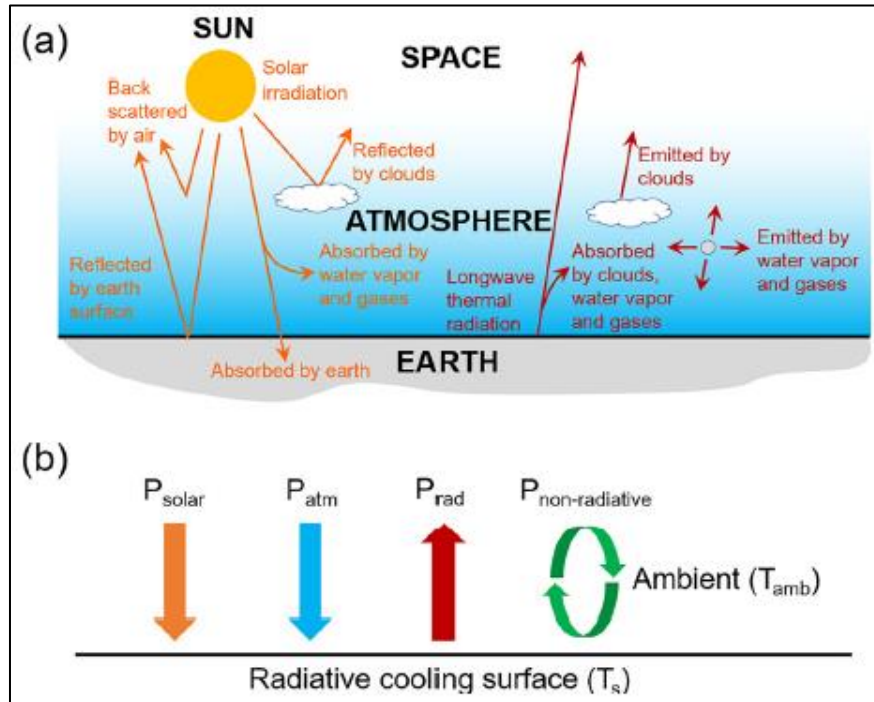
Figure 2.1: Interaction of environmental radiation with the Earth's atmosphere
(Zhao et al., 2019)

2.1.2   Principles of Radiative Cooling

Generally, planet earth gains energy from the sun as the sun emits solar irradiation. On the other hand, to maintain a balance in energy, the Earth will radiate the same amount of energy. The maximum cooling power of a radiative cooler determines the lowest temperature achievable. Thus, the net cooling power of a radiative cooler can be expressed in the equation below.

$$P_{net} = P_{rad} - P_{atm} - P_{solar} - P_{nonrad} \qquad (2.1)$$

Whereas P_{rad} refers to the thermal radiation power from the surface, P_{atm} refers to atmospheric radiation power absorbed on the surface and P_{solar} refers to solar irradiation absorbed on the surface, an example of P_{nonrad} is convection and conduction which are non-radiative heat transfer between surrounding and surface of the cooling material. Effects from the surroundings are neglected in the equation above, for instance, buildings. For applications of radiative cooling used during the night, normally absorption of solar irradiation is not a concern. However, for applications that use radiative cooling during the

daytime whereby the device is exposed to the sun, solar absorption of the material used for the surface must be taken into consideration. Daytime radiative cooling was enabled by recent developments in photonic designs.

Radiative cooling is a form of the passive cooling system which requires no external energy source to operate (Zhao et al., 2018). Radiative cooling has been recognised to be a crucial technology for energy efficiency and energy harvesting applications. In the 21st century, the global energy demand for air conditioning and refrigeration has been increasing dramatically. Many factors contribute to this matter for instance global warming, and population growth not to mention industrial development too. The current technology for cooling systems brings several negative effects on the environment such as hydrofluorocarbons (HFC) being released into the environment which raises the concern of many individuals. Efforts had been made to create a cooling system that does not cause environmental damage and is efficient at the same time.

2.1.3   Factors affecting Radiative Cooling

Primarily, atmospheric radiation comes from various sources which consist of molecules and aerosol particles. For instance, oxygen (O_2), carbon dioxide (CO_2), and ozone (O_3). The emissivity of the atmosphere is displayed in Figure 2.2. From Figure 2.2, different molecules exhibit different emissivity at different wavelengths. For example, O_3 has a narrow emission band around the wavelength of 9.6 µm. On the contrary, carbon dioxide (CO_2) displayed a broad emission band in Figure 2.2. The sun is a blackbody that emits radiation and sunlight rays will travel from the sun and pass through the atmosphere. However, attenuation of the sunlight will occur because of scattering and absorption by particles and molecules in the atmosphere. This indicates that as the sunlight passes through more atmosphere, the greater the attenuation of sunlight (Zhao et al., 2019). Moreover, atmospheric emissivity can be affected by various factors, for example, aerosol, day-night effect, seasons, the humidity of the air, and more. The humidity of the air refers to the amount of water content in the atmosphere. This is a factor that can affect atmospheric emissivity, the amount of water content within the atmosphere can be referred to as "precipitable water" (PW). The definition of PW is the depth of water in a column whereby the water

is precipitated as rain (Zhao et al., 2019). Figure 2.3a shows the relation of the PW levels with atmospheric emissivity whereby the PW levels are 1.5cm, 3cm, and 6cm. Figure 2.3a also displays a trend showing as PW increases, atmospheric emissivity increases. Thus, radiative cooling power is reduced when there is water vapour present in the atmosphere (Zhao et al., 2019).
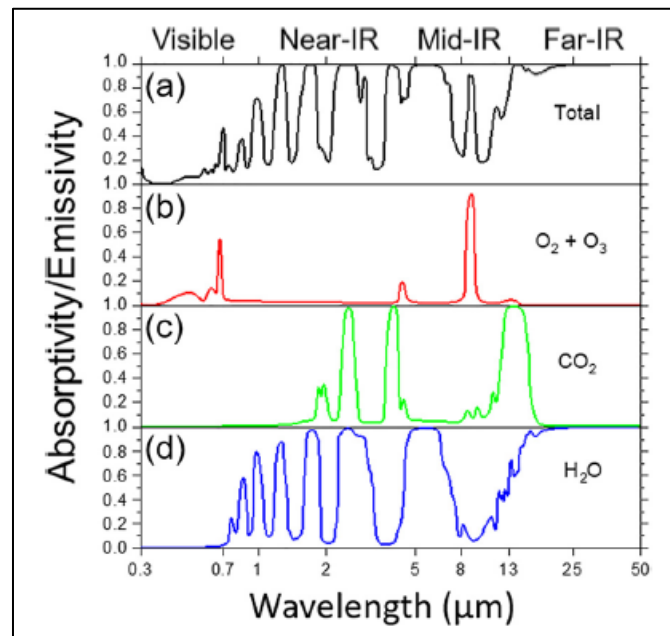
Figure 2.2: Emissivity of different gases in the atmosphere across the range of wavelength from 0.3 to 50 µm (Zhao et al., 2019)
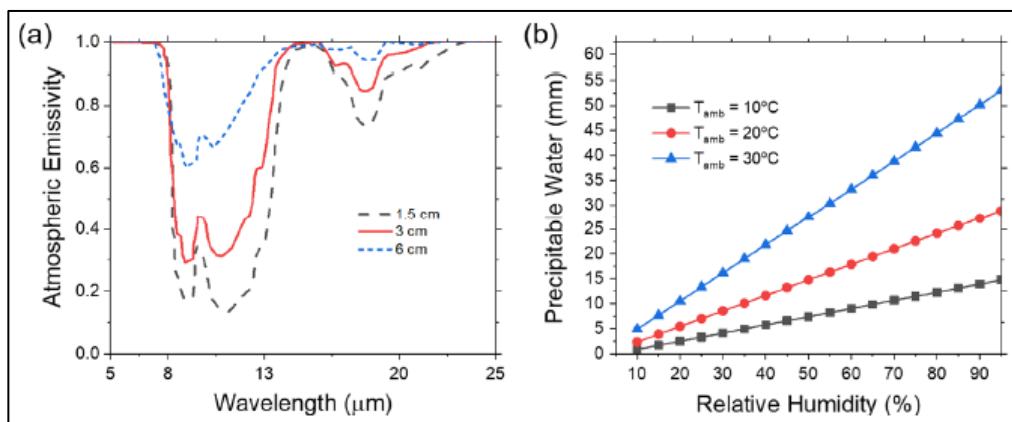
Figure 2.3: Relation of humidity and atmospheric emissivity (Zhao et al., 2019)

Furthermore, clouds in the sky are also another factor that will affect atmospheric radiation. Oftentimes, clouds can be seen covering the skies during the day. Not to mention that clouds come in different types for insta cirrus and stratus, Figure 2.4 shows an illustration of the types of clouds. Atmospheric radiation can be affected by the cloud type, altitudes of clouds, cloud thickness, and cloud compositions also clouds continuously change their behaviours over time. An experiment had been conducted and the results shown in Figure 2.5 show that net radiative cooling power reduction can be related to cloud cover fraction as it increases. However, in the experiment certain aspects were neglected such as the height of the clouds, thickness of the clouds, and the observation angle of the radiative cooling surface. Thus, the experiment displays the effect of the cloud cover fraction. From Figure 2.5, it can be seen that a net radiative cooling power of 98 W/m^2 is achieved on a clear skies condition and with a sky condition that has an overcast cloud produces a net radiative cooling power of 5 W/m^2.
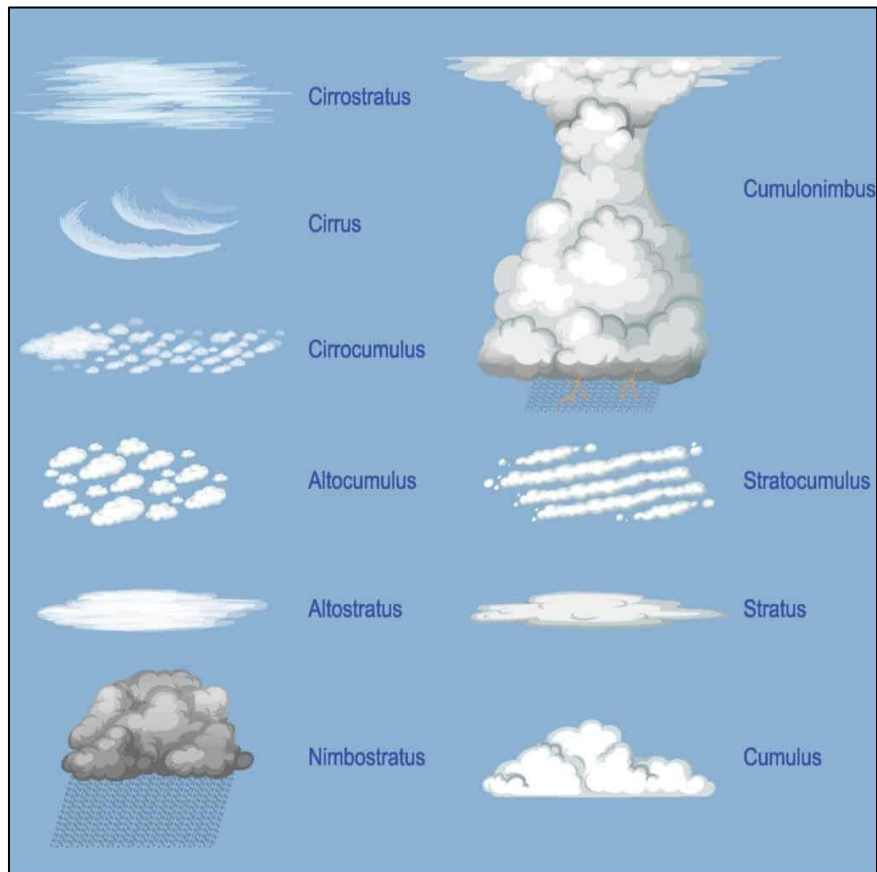
Figure 2.4: Types of clouds (Types of Clouds: Discover the 4 Main Cloud Groups, 2022)
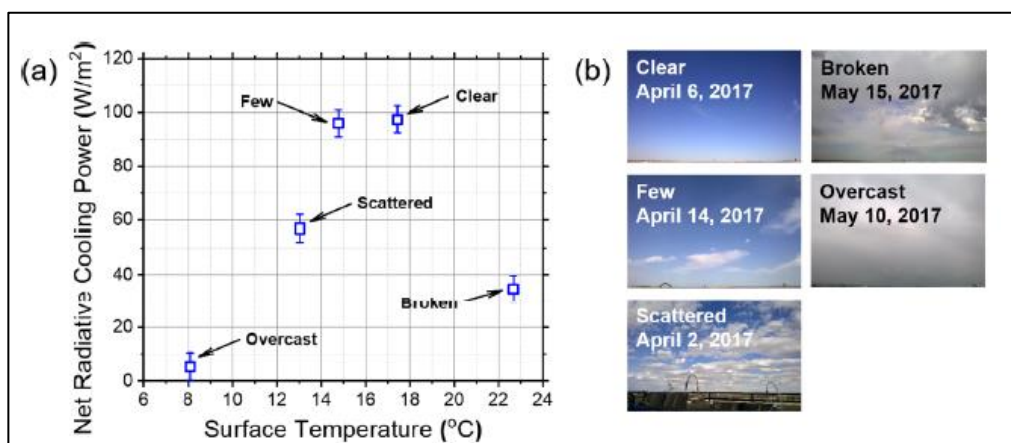
Figure 2.5: (a) Different net radiative cooling power and surface temperatures (b) Cloud coverage on different days (Zhao et al., 2019)

2.2 Materials used for Radiative Cooling

To efficiently achieve the highest cooling power and achieve the lowest temperature, many materials had been studied and investigated to be utilized in a radiative cooler. Materials with different properties will display different effects when used in a radiative cooler. This is because different materials have different emissivity and behave differently from one another. When considering radiative cooling during the night-time, absorption of solar irradiation and solar reflectance are not to be considered. However, due to advancements in technology, daytime radiative cooling can be achieved as well, but certain parameters need to be considered too.

To achieve efficient radiative cooling, many materials were studied for the realization of the potential of radiative cooling. For instance, polymer films, white pigmented paints, silicon monoxide (SiO) films, and more (Hossain and Gu, 2016). Polyvinyl-fluoride polymer film (TEDLAR) was used by Catalanotti et al. and Bartoli et al as a radiative emitter. However, this material was not that efficient as there was infrared radiation (IR) absorption detected beyond the 20 µm wavelength and many absorption peaks were found at wavelengths smaller than 8 µm. Another study was conducted for white paint containing titanium dioxide (TiO_2). The paint was used to coat aluminium plates and then the plates were used as IR radiators. It was found that a steady cooling of 10 °C below ambient temperature happened at night under the conditions of clear skies (Hossain and Gu, 2016). However, the IR radiator did not achieve realistic cooling under direct sunlight at noontime.

2.2.1 Mixture of titanium dioxide (TiO_2) and silicon dioxide (SiO_2) particles in a single-layer radiative cooling coating

A study had been conducted using a radiative cooling coating that consists of a mixture of titanium dioxide (TiO_2) and silicon dioxide (SiO_2) particles. Figure 2.6 shows the illustration of the coating used. Based on the figure, the mixture of TiO_2 and SiO_2 particles were embedded in a radiative cooling coating which the use of the particles is for reflection of solar irradiation and to emit radiation through the atmospheric window. There are several reasons why TiO_2 and SiO_2 were chosen for this experiment, one of them being that TiO_2 can act as

reflective material to reflect solar irradiation, and the extinction coefficient for TiO_2 increases as the wavelength reaches larger than 10 µm indicating the emissivity of TiO_2 is high in this specific spectrum. SiO_2 on the other hand has a large extinction coefficient at the "atmospheric window" (Cheng et al., 2020). However, in the 10 to 12 µm wavelength spectrum, SiO_2 has a decrease in emissivity which will affect the effectiveness of the radiative cooling coating. Thus, TiO_2 particles will be supplementary to increase the emissivity. In the experiment, the single-layer radiative cooling coating is also defined as a semi-transparent medium having multi-particle systems with non-uniform size distribution.

Due to the coating consisting of a mixture of 2 particles, volume fraction plays a role in the efficiency of the coating. It was found that TiO_2 with a volume fraction of 5% and SiO_2 with a volume fraction of 5.5% displayed the best radiative cooling performance (Cheng et al., 2020). Having said that the thickness of the coating is 200 µm and the diameter for TiO_2 and SiO_2 particles are 0.4 µm and 5.0 µm respectively. Furthermore, for this single-layer radiative cooling coating, the average reflectivity can achieve 95.6% and the average emissivity in the "atmospheric window" can achieve 94.9%.
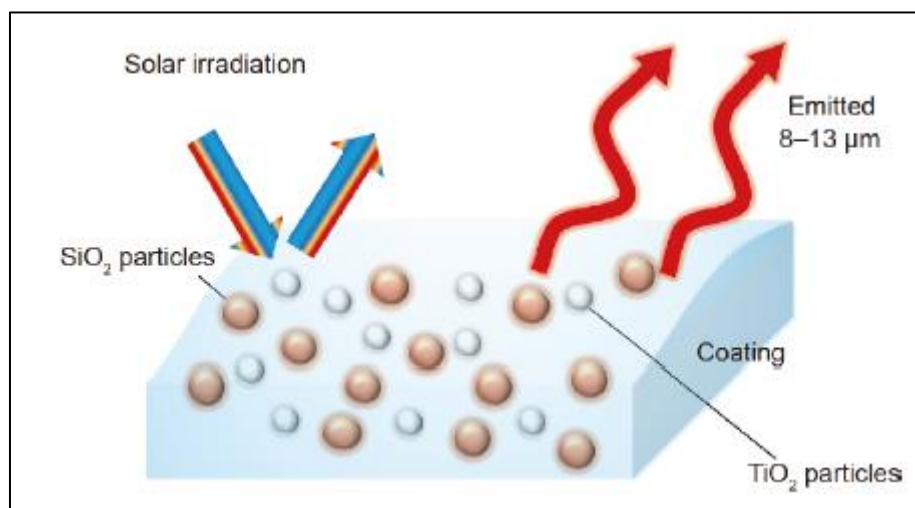
Figure 2.6: Radiative cooling coating that consists of a mixture of SiO2 and TiO2 (Cheng et al., 2020)

2.2.2   Nanophotonic structures

A photonic device was reported to cause a reduction in the temperature of 4.9 °C below ambient temperature. This device consisted of 7 alternating layers that contains hafnium oxide (HfO_2) and silicon dioxide (SiO_2) with different thicknesses. Figure 2.7a shows the composition of the device whereby the thicker layers which make the top 3 layers contributes to IR emissivity and the bottom 4 thinner layer are able to achieve a maximum of 97% solar reflection. The device was found to have achieved a cooling power of 40.1 W m^{-2} at ambient temperature while under direct sunlight and with proper convective or conductive shielding (Hussain and Gu., 2016). Furthermore, Figure 2.7b shows the emissivity across different wavelengths of the device. It is shown that the IR emission of the device from the 8 µm to 13 µm range is not very strong.
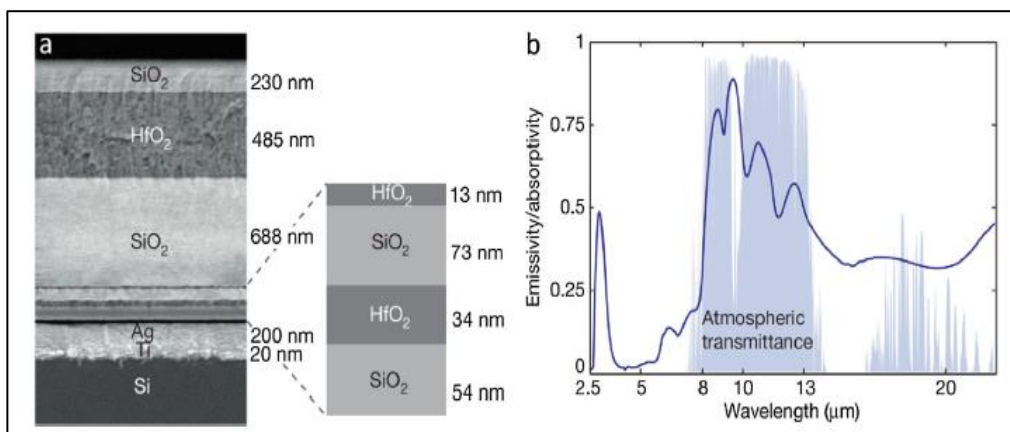
Figure 2.7: a) Electron microscope image of radiative cooling device b) Measured emissivity of the radiative cooler at a 5° angle of incidence with the atmospheric window in the background (Hussain and Gu, 2016)

Furthermore, another researcher used a thermal emitter with a design that consists of multilayer conical metamaterial pillar arrays. Each pillar is made of different layers of aluminium and germanium whereby aluminium, and germanium have a thickness of 30 nm and 110 nm respectively. Figure 2.7b shows high emissivity at 8 to 13 µm wavelength and outside of the atmospheric window the emissivity is low. The emitter can achieve a value of 116.6 W/m^2 for radiative cooling power at ambient temperature (Zhao et al., 2018). Not to

mention that by using a solar reflector, solar absorption can be reduced to 3%. The structure of the pillars and the emissivity of the emitter is shown in Figure 2.8a and Figure 2.8b respectively.
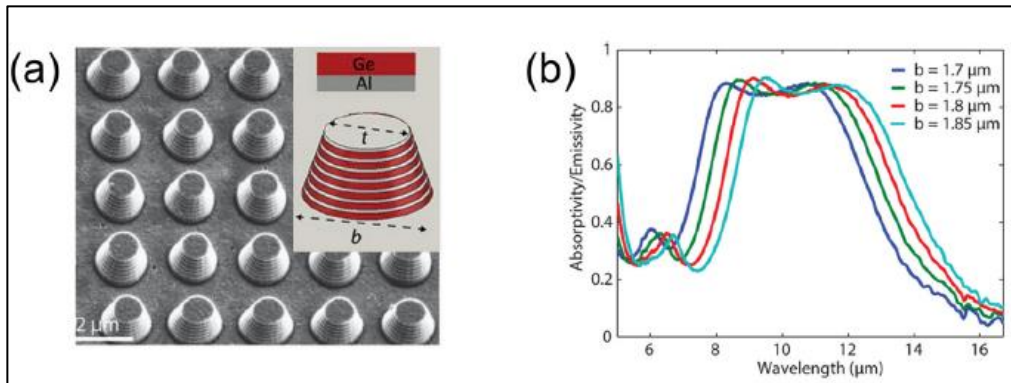
Figure 2.8: (a) Structure of the pillar made of different layers of aluminium and germanium (b) Emissivity of the radiative emitter (Zhao et al., 2018)

2.2.3 Polymer-based materials

Polymeric coatings can be used in a radiative cooler as well. Polymeric coatings have a polymer matrix that also contains dielectric particles that act as fillers which are also randomly distributed. There are a few examples of polymers such as polyvinyl chloride (PVC), polydimethylsiloxane (PDMS), polymethyl methacrylate (PMMA), polyvinylidene fluoride (PVDF), polymethyl pentene (TPX), and many more. Polymers can be used for radiative cooler coatings due to their properties of low solar absorption and high thermal emissivity. In a study conducted, PDMS was selected because it has a lower refractive index and strong emissivity within the atmospheric window. To boost solar reflectivity, nano-sized dielectric fillers can do that through Mie scattering. In this study, TiO_2 was chosen as the filler (Fu et al., 2021). Due to the sedimentation effect, there are 4 different gradient distributions of particles obtained, whereby there is the density-gradient and size-gradient as shown in Figure 2.9. The modified Monte-Carlo method was used in this experiment to calculate parameters such as solar reflectance and infrared emittance for the density-gradient coating. The best cooling performance shown was that one having the highest volume fraction whereby $f_{top} = f_{bot} = 0.3$. Furthermore, an upward density-gradient

coating is better than a downward gradient coating in terms of solar reflectance due to the sunlight can be scattered more efficiently at the top boundary that has a higher volume fraction of TiO_2.

Moving on, the downward size gradient displays better solar reflectivity and considerable infrared emissivity. Compared to a randomly distributed structure, the downward size gradient has an extra cooling power up to about 36 W/m^2 due to the solar reflectivity being higher. Through this study, it can be understood that light interacts with the particles at the top of the coating first as well as smaller particles scatter sunlight more efficiently (Yang et al., 2021).

Another research was conducted by using a PVC film with a thickness of 12.5 µm with an aluminium back coating (Zhao et al., 2018). The setting of the experiment was that the radiative cooler was placed into a box that is thermally insulated with a cover made of infrared transparent PE film. The radiative cooler had a 15 °C sub-ambient temperature cooling.
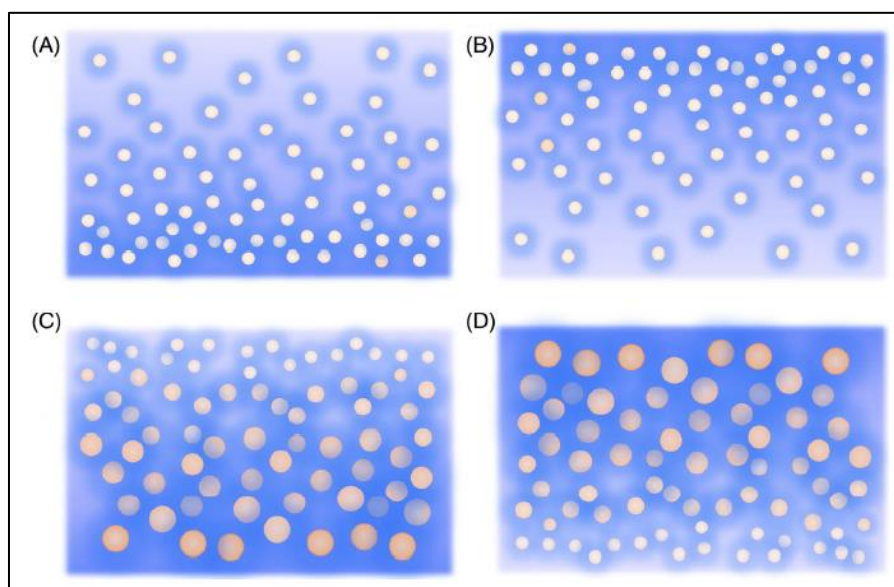
Figure 2.9: Schematics of different gradient structures (a) downward density-gradient (b) upward density-gradient (c) downward size gradient (d) upward size gradient (Fu et al., 2021)

2.3   Radiative Cooling with thermoelectric for power generation

In order to generate power through the thermoelectric effect, a temperature gradient has to be present between the hot side and the cold side. The larger the temperature gradient, the higher the power generated. Basically, the Seebeck effect is involved in thermoelectric power generation. In a thermoelectric module, a hot side and cold side are present. In this case, a passive cooling system which is radiative cooling is used for the cold side. Generally, radiative cooling occurs when an object radiates thermal radiation through an atmospheric window into outer space which acts as a cold sink. Normally, radiative cooling can have the best cooling performance during night-time and when the sky is clear. But many efforts had been done to achieve radiative cooling during daytime. Radiative cooling can be achieved during the day and night by equipping advanced surface designs. A certain material can be used to minimize solar absorption during the day that also has a strong solar reflectance. Not to mention that the material has to have high emissivity within the atmospheric window to achieve the best cooling performance.

Research had been conducted to prove that radiative cooling can be used for thermoelectric power generation continuously through day and night. In the research, a wavelength-selective emitter (SE) which is made from a glass substrate and a 100 nm thickness aluminium (Al) thin film was used (Ishii et al., 2020). Other than that, a broadband emitter (BE) was chosen as a control sample which is a blackbody paint-coated glass substrate. Both SE and BE were attached to a thermoelectric device. Figure 2.10a shows the illustration of the setup, Figure 2.10b shows a photo of the actual samples taken outdoors, and Figure 2.10c shows the thermograph that was taken for both samples.
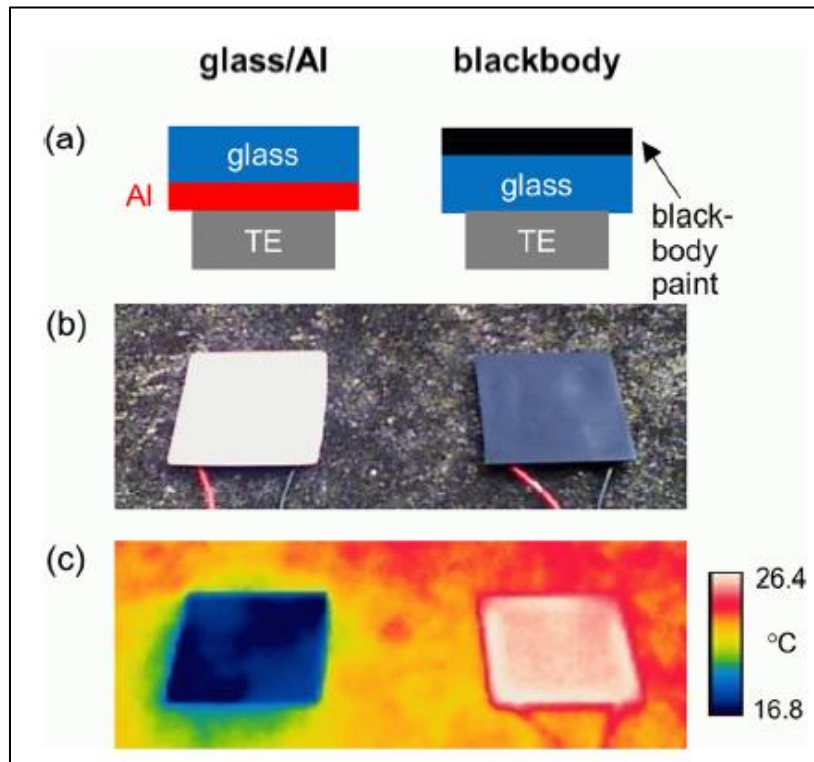
Figure 2.10: (a) Illustration of the experimental setup (b) Photos of the
actual samples taken outdoors (c) Thermograph taken for
both samples (Ishii et al., 2020)

Through the research, it was found that the glass/Al sample has an emissivity that is near to unity in the MIR range as shown in Figure 2.11a. Not only that, the glass/Al sample also had a high solar reflectivity in the 0.3 to 2.5 μm wavelength which is also shown in Figure 2.11b.
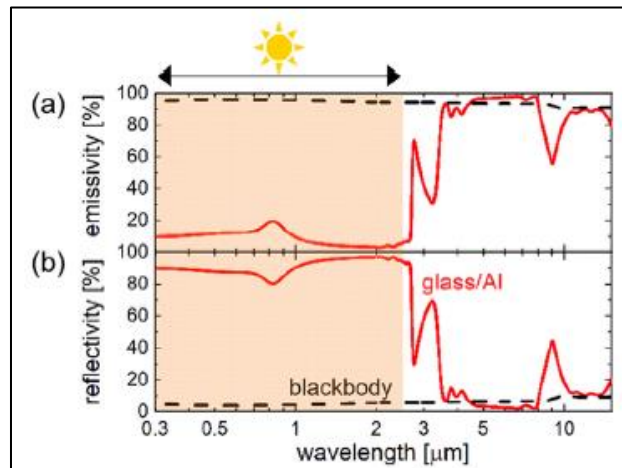
Figure 2.11:   (a) Emissivity of glass/Al sample (b) Reflectivity of glass/Al sample (Ishii et al, 2020)

After that, TE voltage was recorded for both samples and shown in Figure 2.12. Moreover, the glass/Al sample generated TE voltage throughout the whole day without the value of TE voltage reaching zero, which proves that the sample can generate power continuously throughout the day and night by utilizing the concept of radiative cooling. Referring to Figure 2.12 whereby the TE voltage for the blackbody sample had crossed zero a few times. The crossing was due to the temperature on top being higher than the temperature at the bottom in the morning and the other way around during the night. From the results obtained, the glass/Al sample had a maximum temperature difference of +5 K and the blackbody sample had -15K. The glass/Al sample managed to generate a maximum TE voltage of 30 mV based on Figure 2.12. This experiment proved that an SE can be cooled through radiative cooling and using a TE module the temperature difference can be used to generate power continuously during day and night time.
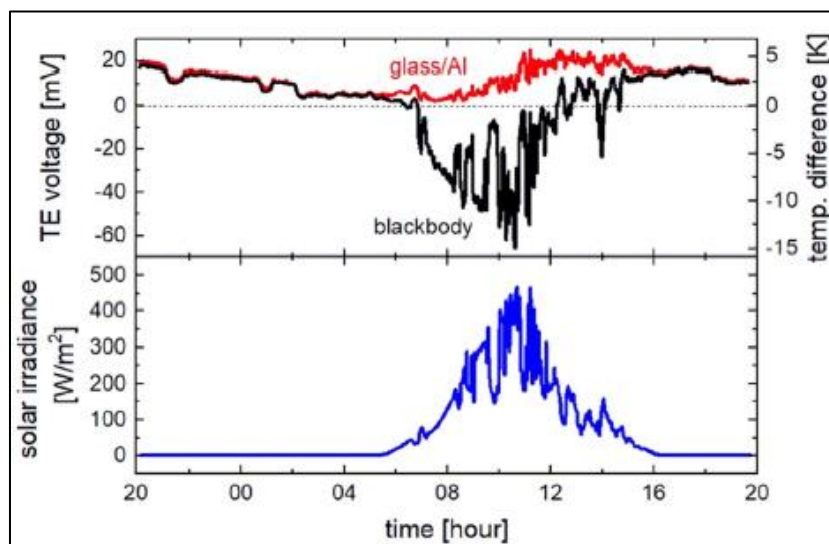
Figure 2.12:   (a) TE voltage generated and temperature difference (b) Solar irradiance measured (Ishii et al., 2020)

2.4   Summary

Radiative cooling occurs when an object emits thermal radiation through an atmospheric window within the 8 µm to 13 µm wavelength into outer space which acts as a thermal reservoir. There are several applications for radiative cooling. One of the applications is using radiative cooling with thermoelectric for power generation.

Furthermore, there are several factors that could affect the efficiency of radiative cooling. For instance, molecules and aerosol particles found in the atmosphere, clouds, day-night effects, and humidity. Not to mention many materials can be used for radiative cooling, there is a mixture between silicon dioxide (SiO_2) and titanium dioxide (TiO_2), nanophotonic structure and poly-based materials. Different materials displayed different cooling results, efficiencies and properties when used for radiative cooling. Some included complex preparation steps, and some can be prepared easily and a low cost. Not to mention that some materials consist of multiple layers of different materials.

Moreover, there is one more material that could be used as a radiative cooling material, which is a thin aluminium (Al) film. This particular material is low-cost and easily sourceable in the market.

CHAPTER 3

METHODOLOGY

3.1   Introduction

This chapter outlines 4 sections which consist of (i) materials used for this project (ii) sample and coating preparations method (iii) experiment test methods (iv) experiment setup. The first section highlights the materials that are crucial and needed for this experiment and the properties of the materials are specified. The second section describes how the samples were prepared and the method used to prepare the coating for radiative cooling. The third section then describes methods and experiment procedures to test the samples prepared for the analysis of the materials used. Then lastly the fourth section elaborates on prototype design as well as a detailed setup of the experiment to obtain data. This chapter elaborates on how the project was carried out, the design of the experiment and the flow of the whole project. The main objective of this project is to create a prototype that can generate power through radiative cooling. The flowchart of the project is shown in Figure 3.1.

Materials Preparation

- Silicon Dioxide (SiO₂) powder
- Titanium Dioxide (TiO₂) powder
- Polyvinyl Alcohol (PVA)
- Isopropyl Alcohol
- Distilled Water
- Thermal Grease

Mixture for coating and samples preparation

SiO₂ mixture

SiO₂ powder and isopropyl alcohol were mixed and stirred at 400 r/min for 1 hour. Then added with PVA that was mixed with distilled water and stirred at 150 r/min for 1 hour.

TiO₂ mixture

TiO₂ powder and isopropyl alcohol were mixed and stirred at 400 r/min for 1 hour.

Experimental procedures and tests

XRD

Diffraction patterns of the SiO₂ and TiO₂ samples were analysed. Samples included in the test were SiO₂ powder, SiO₂ coating, TiO₂ powder and TiO₂ coating.

SEM

SiO₂ and TiO₂ coatings were examined under high magnification to examine the surface morphology of the coatings.

EDX

Compositions of the SiO₂ and TiO₂ sample coatings were analysed.

Samples preparation and coating process

Samples for SiO₂ and TiO₂

The SiO₂ and TiO₂ suspensions were each deposited on microscope glass by using a dropper.

Coating process

Each layer of coating was coated onto the TEG modules using the bar coating method with the thickness set to 150 μm. 4 TEG modules were coated with single layer SiO₂ coating, 4 TEG modules were coated with single layer TiO₂ coating and 4 TEG modules were coated with single layer SiO₂ coating as the bottom layer and single layer TiO₂ coating as the top layer.

Experimental Setup

Holders for the TEG modules and aluminium heatsinks were prepared and the material selected was plywood with a thickness of 30mm. Heatsinks were force-fitted into the holes craved and thermal grease was applied on top of the heatsinks. TEG modules were then attached to the heatsinks with the radiative coating facing upwards.

Data collection

The TEG modules were exposed under the sky and data was collected over the course of 24 hours.

Figure 3.1: Flowchart diagram of methodology section

3.2 Materials and Chemicals

3.2.1 Chemical Components

The list of chemical components needed to conduct the research experiment is listed and shown in Table 3.1.

Table 3.1: List of chemical components

Chemical Components	Applications	Sources/Suppliers
Silicon Dioxide (SiO_2) powder	Radiative cooling coating	Outsource
Titanium Dioxide (TiO_2) powder	Radiative cooling coating	Outsource
Polyvinyl alcohol (PVA)	Binder	Outsource
Isopropyl Alcohol	Solvent	UTAR
Distilled water	Solvent	UTAR
Thermal Grease	To promote better heat conduction between TEG modules and aluminium heat sinks	Outsource

3.2.2 Materials

The list of materials needed to conduct the research experiment is listed and shown in Table 3.2.

Table 3.2: List of Materials

Materials	Application	Quantity
Plywood	Prototype of the experiment	1
Polyethylene (PE) film	Protective layer	1
Aluminium Heatsink	To serve as a heat reservoir	1

3.3   Apparatus and Equipment

The list of apparatus and equipment needed to conduct the research experiment are listed and shown in Table 3.3.

Table 3.3:   List of Apparatus and Equipment

Apparatus/Equipment	Application	Quantity
Magnetic stirrer	To stir a mixture with desired speed and temperature	1
Bar coating machine	To coat suspension onto a substrate	1
Infrared thermometer	To measure the temperature of a surface	1
Weighing machine	To weigh the weight of the materials needed	1
Thermoelectric (TEG) module (Tec1-12706)	To generate power	1
Thermocouple	To measure temperature	1
Wood cutting tool	To cut pieces of wood into desired shape and size	1
Wood carving tool	To carve out the desired shape on a piece of wood	1
Digital Multimeter	To obtain voltage readings	1
X-ray Diffraction (XRD)	To analyse the structure of materials	1
Scanning Electron Microscope (SEM) with Energy Dispersive X-ray (EDX)	To analyse the surface morphology and elemental compositions of materials	1
Hot glue gun	To join parts and fix them together	1

3.4   Sample and Coating preparation

In this project, 4 samples were required for the X-ray diffraction (XRD) test and 2 samples were required for the scanning electron microscopy (SEM) and energy dispersive X-ray spectroscopy (EDX) test.

To generate power with radiative cooling, coatings of radiative material were required to be coated on the thermoelectric generator (TEG) module and the TEG modules used are the Tec1-12706 model. In this project, titanium dioxide (TiO_2) and silicon dioxide (SiO_2) are chosen as materials used for the coatings. Coatings can be differentiated into single-layered coating and double-layered coatings. Single-layered coatings consist of single-layer SiO_2 coating and single-layer TiO_2 coating. On the other hand, the double-layered coating is a coating that consists of SiO_2 coating on the bottom layer and TiO_2 coating on the top layer. An illustration of the TEG modules and the coatings is shown in Figure 3.2. The dimensions of the TEG module are 40 mm×40mm×3.8mm.
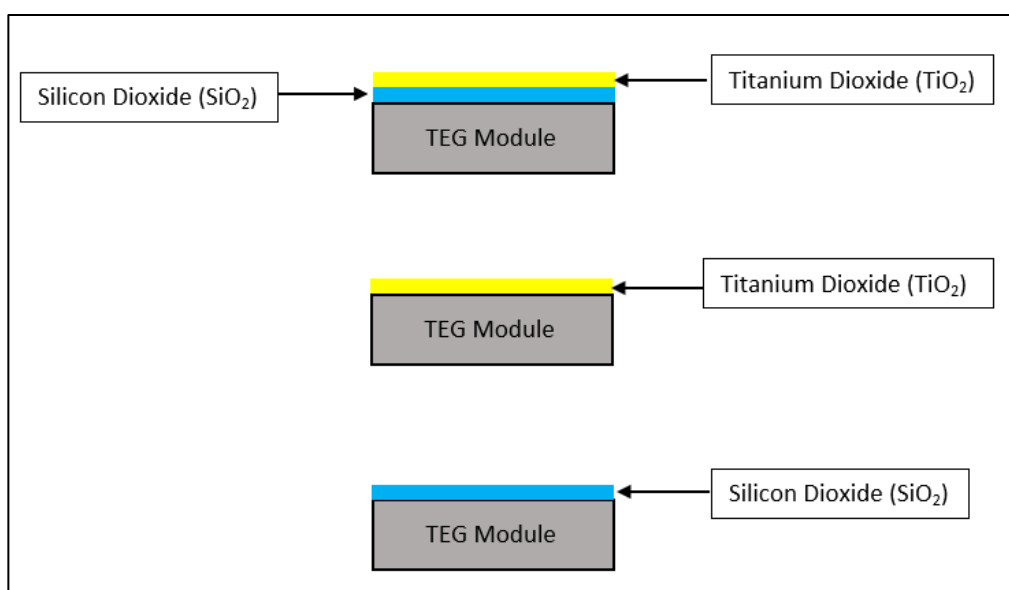
Figure 3.2: Illustrations of coatings on TEG modules

3.4.1 Silicon Dioxide (SiO_2) sample and coating preparation

Generally, the same sample can be used for both XRD and SEM-EDX tests. However, the test sequence must be followed with the XRD test and then the SEM-EDX test.

The same solution was used for the sample and the coating on the TEG module. Firstly, SiO_2 powder was adopted to prepare the mixture. In the first step of preparing the mixture, the mixture was prepared by mixing the SiO_2 powder with isopropyl alcohol. The volume ratio between powder and solvent

is 1:1. The mixture was stirred on a stirrer at 400 r/min for 1 hour in order to obtain a uniform suspension. Furthermore, PVA was used as a binder for the mixture. The volume ratio for PVA powder to distilled water is 1:10. To prevent bubbles from forming in the PVA solution, the solution must be stirred at a low speed which is non-turbulent. Thus, the solution was stirred on a stirrer at 150 r/min for 1.5 hours. Once both mixtures are done stirring, the PVA solution was then added to the SiO_2 mixture.

For the sample needed for the XRD test and SEM-EDX test, the suspension is deposited on a piece of microscope glass using a dropper. Beforehand, the piece of microscope glass was cleaned with liquid detergent and rinsed with distilled water to wash and clean away any impurities and residues. Once deposited, the sample was left to dry at room temperature for 2 hours.

Moving on to the preparation for the SiO_2 coating on the TEG modules. In this step, 8 pieces of the TEG module are required to be coated. As for the coating method, the bar coating method was chosen due to its simplicity, and availability of the machine and using this method allows uniform coating. The bar coating machine used was the JR-400D Auto Film Machine manufactured by Shanghai Jiuran Instrument Equipment Co., Ltd shown in Figure 3.3. The bar had 4 different thickness options; for this project, the thickness of SiO_2 coating is 150 µm. The suspension was deposited on the one end of the TEG module and the bar was pushed one end to the other end which then completed the coating process. The coating was then left to dry at room temperature for 2 hours.

3.4.2 Titanium Dioxide (TiO₂) sample and coating preparation

In the section, the preparation method is almost similar to the SiO_2 coating. The difference is that for this coating there is no binder required.

The same solution was used for the sample and the coating on the TEG module. Firstly, TiO_2 powder was adopted to prepare the mixture. In the first step of preparing the mixture, the mixture was prepared by mixing the TiO_2 powder with isopropyl alcohol. The volume ratio between powder and solvent is 1:3. The mixture was stirred on a stirrer at 400 r/min for 1 hour to obtain a

uniform suspension. Once the mixture was done stirring, it was then used for the sample and coating preparation.

For the sample needed for the XRD test and SEM-EDX test, the suspension was deposited on a piece of microscope glass using a dropper. Beforehand, the piece of microscope glass is cleaned with liquid detergent and rinsed with distilled water to wash away any impurities and residues. Once deposited, the sample was left to dry at room temperature for 2 hours.

For the TiO_2 coating, the suspension was deposited on 4 pieces of TEG modules that had SiO_2 coating deposited on them and another 4 pieces of TEG modules without any coating deposited on them. The coating method adopted was the bar coating method as it is easy to use and thickness control is achievable. The machine used for the coating was the JR-400D Auto Film Machine manufactured by Shanghai Jiuran Instrument Equipment Co., Ltd shown in figure 3.3. TiO_2 was then coated onto the TEG modules with a thickness of 150 µm. Once the coating process was completed, the coatings on the TEG modules were left to dry at room temperature for 2 hours.
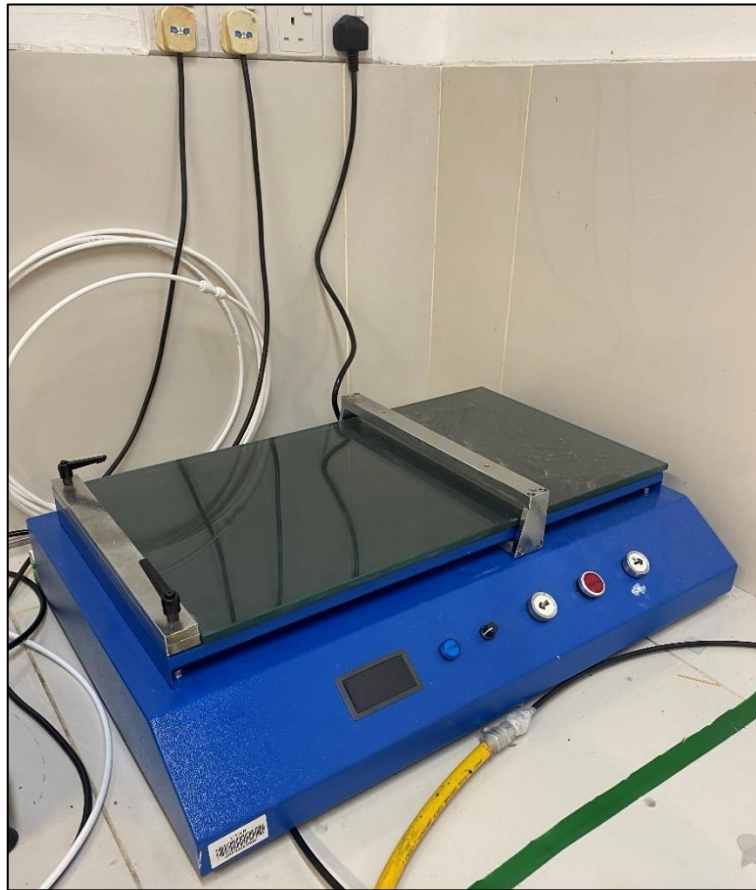
Figure 3.3: JR-400D Auto Film Machine

Figure 3.4: (a) Bar (b) Thickness options

3.5   Experimental Test Methods

In this project, the X-ray diffractometer (XRD) and scanning electron microscopy (SEM) and energy dispersive X-ray spectroscopy (EDX) test were required to analyse the SiO_2 and TiO_2 particles.

3.5.1   X-ray Diffraction (XRD)

SiO_2 powder, SiO_2 sample, TiO_2 powder and TiO_2 powder were characterised through XRD. The X-ray diffractometer model XRD-6000 manufactured by Shimadzu from Japan as shown in Figure 3.5 was used. The analysis of XRD was performed between the range of $10°$ to $70°$ (2θ) with a scan speed of 2 deg/min. The test period for each sample took approximately 30 minutes. Then, the diffraction patterns of the samples were analysed.

Moulds shown in Figure 3.6 were used to fit in the SiO_2 powder and TiO_2 powder. Furthermore, the SiO_2 sample and TiO_2 sample were fitted into another mould shown in Figure 3.7 and pressed down using a manual pellet press as shown in Figure 3.8 to ensure that the samples will not drop due to gravity during the test period.

Figure 3.5: Shimadzu XRD-6000 X-ray Diffractometer

Figure 3.6: Mould for SiO_2 and TiO_2 powder

Figure 3.7: Mould for SiO_2 and TiO_2 samples

Figure 3.8:   Manual Pellet Press

3.5.2 Scanning Electron Microscope (SEM) test and Energy Dispersive X-ray test

The SiO_2 sample and TiO_2 sample were examined under the scanning electron microscope (SEM). The model of the SEM machine used is the Hitachi S3400-N scanning electron microscope from Hitachi, Tokyo, Japan which is shown in Figure 3.9. SEM was conducted to analyse the surface morphology of the SiO_2 and TiO_2 samples. The samples were stuck onto a holder shown in Figure 3.10 by using carbon tape.

Before the samples were inserted into the machine, the samples were sputter coated with an ultra-thin layer of gold film, which functions to induce thermal conductivity and secondary electron emissions. The sputtering machine used is shown in Figure 3.11. Once the sputter coating process was completed, the samples were inserted into the machine for examination.

After taking images of the SiO_2 and TiO_2 samples using the SEM machine, the next step was to perform the energy dispersive X-ray spectroscopy (EDX) test. The purpose of performing the EDX test on the samples was to identify the elemental composition of the materials.

Figure 3.9: Hitachi S3400-N SEM-EDX Machine

Figure 3.10:   Holder for SEM machine

Figure 3.11:   Sputtering Machine

3.6   Experimental Setup

This section explains the setup of the project which includes the materials and apparatus needed for data collection. The experiment was conducted during mid of August 2022. The location of choice was Cheras, Kuala Lumpur. The experiment took two days to complete, one day for the prototype with

SiO$_2$+TiO$_2$ radiative cooling coating and one day for both single-layered radiative cooling coating prototypes.

3.6.1   Preliminary Planning

To begin the project, a holder for the TEG modules and aluminium heatsink is needed. Hence, a model of the holder was drawn out as a draft using SOLIDWORKS for the preliminary planning phase of the prototype. After determining the dimensions of the holder, the materials needed were then prepared and assembled into the final product.

For the holder, few materials were considered, materials considered were plywood and cardboard. Plywood was chosen as the material used for the holder for the TEG modules due to its mechanical strength, cheaper price and can be easily cut into desired shape and size. The plywood wood was cut into 17×17 cm using a woodcutter and was used as the body of the holder. Furthermore, for the base of the holder, 7×3 cm plywood was cut and used as legs for the holder. After that, from the body of the holder, four holes with the dimension of 4cmx4cm were carved out using a wood carving tool. The concept of force fit was adopted in this project for the aluminium heatsinks which justifies that the holes were craved to the exact dimension of the heatsinks. The dimensions of the aluminium sinks are 40×40×20 mm. Moreover, holes were drilled through the body of the holder to allow wires of the TEG modules to pass through. The parts of the holder were assembled using a hot glue gun. After the assembly process, the holder for the prototype was left to dry at room temperature for 2 hours.

3.6.2   Prototype

Using the holder that was prepared, aluminium heatsinks were force-fitted into the holes on the body of the holder. After that, thermal grease was applied on top of each heatsink and spread evenly. TEG modules were then attached on top of the aluminium heatsinks whereby the radiative coatings were facing upwards. The TEG modules were connected in a series connection to serve the purpose of a generator. A thermal couple was attached to one of the heatsinks to obtain a temperature reading of the heatsink and another thermal couple was attached

to the surface of the TEG also for the purpose of obtaining a temperature reading. 4 layers of polyethylene (PE) film were used to wrap around the bottom of the prototype to minimize airflow around the heatsinks as well as to trap the heat inside so that the heatsinks can reach a higher temperature. Not to mention that a single layer of PE film was also used as a cover above the TEG modules. As the prototype needed to be placed under direct sunlight hence, rain and wind can be a factor that affects the data, hence a cover was used to prevent that. The prototype with SiO_2+TiO_2 coating is shown in Figure 3.12, the prototype with SiO_2 coating is shown in Figure 3.13, and the prototype with TiO_2 coating is shown in Figure 3.14.

The prototype with SiO_2 coating was labelled as "Prototype A", the prototype with TiO_2 coating was labelled as "Prototype B" and the prototype with double-layered (SiO_2+TiO_2) radiative cooling coating was labelled as "Prototype C".
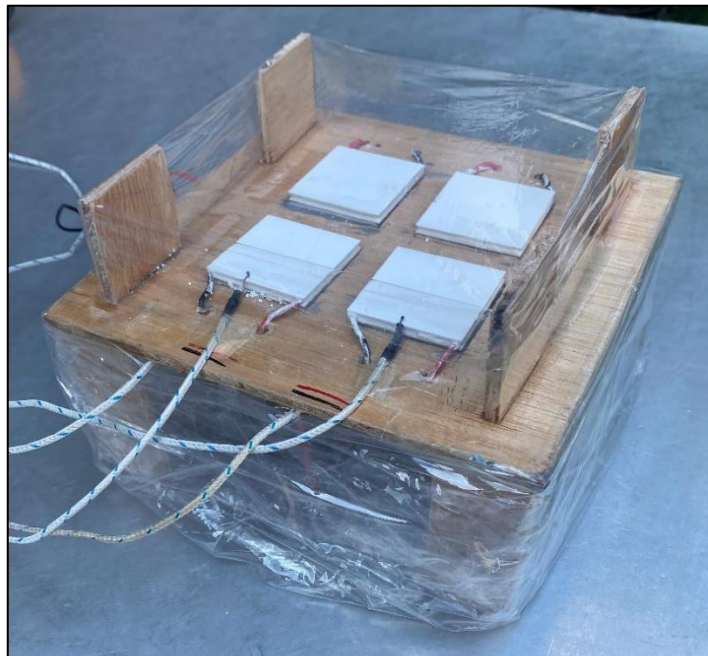
Figure 3.12:   Prototype with SiO_2+TiO_2 coating
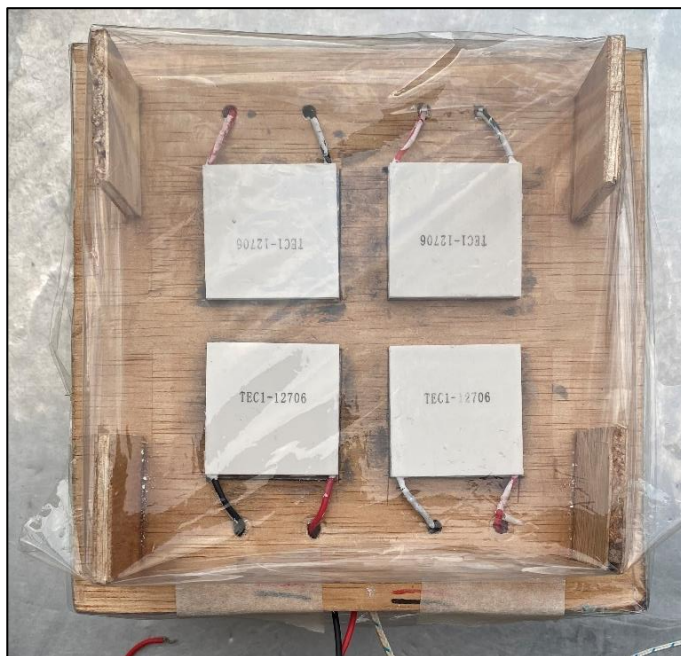
Figure 3.13:   Prototype with SiO$_2$ coating

Figure 3.14:   Prototype with TiO$_2$ coating

3.6.3   Data Collection

Data was required to be collected over 24 hours. Hence, the time for data collection began at 1.00 pm. A digital multimeter was used to obtain the voltage generated by the TEG modules and the thermometer connected to the thermal couples was used to obtain the temperature reading of the heat sinks and the

surface of the TEG modules. An infrared thermometer was also used to cross-check the temperature reading obtained from the thermocouples. Furthermore, thermal images were captured using a thermal imaging camera for each of the prototypes with a different coating to show the cooling effect of the radiative coating. As for the solar irradiance, a solar irradiance meter was used to obtain the reading. During the day of data collection, the conditions of the sky were slightly cloudy constantly across the 24 hours.

3.7   Calculation for Seebeck Coefficient, Maximum Efficiency and Power Generation

A TEG module has to ability to convert heat into electricity according to the Seebeck effect (Yan et al, 2018). Seebeck effect is referring to when there is a temperature difference between the hot and cold ends of the semiconductor material, voltage is then generated (Harun et al,. 2016).

According to research conducted by Harun et al. (2016), the efficiency of thermoelectric materials can be calculated as follows.

$$Z\bar{T} = \frac{\alpha^2 \bar{T}}{kR} \tag{3.1}$$

Where

$Z\bar{T}$ is the figure of merit

α is the Seebeck coefficient

k is the thermal conductivity constant

R is the electrical resistivity

$$\bar{T} = \frac{T_H + T_L}{2} \tag{3.2}$$

Where

T_H is the temperature high

T_L is the temperature low

Hence, based on equations 3.1 and 3.2 the maximum efficiency, η can be calculated assuming that the heat loss is zero.

$$N = \eta_{\text{Carnot}} \left[\frac{\sqrt{1+Z\overline{\overline{T}}}-1}{\sqrt{1+Z\overline{\overline{T}}}+\frac{T_L}{T_H}} \right] \qquad (3.3)$$

Where

η_{carnot} is Carnot efficiency, and can be calculated by,

$$\eta_{carnot} = 1 - \frac{T_L}{T_H} \qquad (3.4)$$

The Seebeck coefficient can be calculated based on the given formula of,

$$\alpha = \frac{\overline{x}\,V}{\overline{x}\,T} \qquad (3.5)$$

Where

$\overline{x}V$ is the average voltage generated

$\overline{x}T$ is the average temperature difference

The magnitudes of voltage generated are affected by the temperature difference of 1 °C across the Peltier device, as stated by the Seebeck effect. According to FerroTec. (n.d.), the output power of the thermoelectric generator in watts can be calculated with the formula,

$$P_o = \frac{NT \times (S_M \times DT)^2}{4 \times R_M} \qquad (3.6)$$

Where

NT is the total number of TEG modules

S_M is the TEG module's average Seebeck coefficient in volts/°K

DT is the temperature difference

R_M is the TEG module's average resistance in ohms

3.8   Summary

As a summary for the methodology section, SiO_2 and TiO_2 were used as materials for radiative cooling. Samples of SiO_2 and TiO_2 were analysed using scanning electron microscope (SEM), energy dispersive X-ray (EDX), and X-ray diffraction (XRD). After that, the models of the prototypes were developed using plywood and the prototypes were setup accordingly. Three prototypes were developed for the experiment, whereby the prototypes were labelled as prototype A, prototype B, and prototype C. Prototype A consist of a single-layer SiO_2 coating, prototype B consist of a single-layer TiO_2 coating, and prototype C consist of a double-layer coating with SiO_2 as the bottom layer and TiO_2 as the top layer. After the prototypes were developed, they were placed directly under the sky for the experimental setup. Data collection was done over the course of 24 hours. Once all the data were collected, the calculation steps were performed to obtain the Seebeck coefficient, maximum efficiency and the power generated.

CHAPTER 4

RESULTS AND DISCUSSION

4.1 Introduction

In this chapter, it starts with the results and discussion part of the characterisation of the properties of both coatings which are the silicon dioxide (SiO_2) and titanium dioxide (TiO_2) radiative cooling coatings characterised via X-ray diffraction analysis (XRD), scanning electron microscopy (SEM), and energy dispersive X-ray spectroscopy (EDX). After that, the following section presents analyses and discussions of the results obtained after leaving the prototype models of the radiative cooling-thermoelectric generator under the sky for 24 hours.

4.2 Characterisation of Silicon Dioxide (SiO_2) and Titanium Dioxide (TiO_2) with Scanning Electron Microscope (SEM) and Energy Dispersive X-ray (EDX)

In this section, both SiO_2 and TiO_2 samples were analysed with scanning electron microscope (SEM) and energy dispersive X-ray (EDX). The purpose of using the SEM was to evaluate the surface of the materials and the purpose of EDX was to identify the elemental composition of materials.

4.2.1 Scanning Electron Microscope (SEM)

The SEM images of SiO_2 and TiO_2 were obtained from the SEM-EDX machine and shown in Figure 4.1 and Figure 4.2 respectively. The SiO_2 coating was investigated at magnifications of $\times 2000$ whereas the TiO_2 coating was investigated at magnifications of $\times 5000$. Different magnification values were used for both coatings, the purpose of it was to obtain a clearer image of the surface of the coatings. The image of the SiO_2 appeared to be more of a crystalline structure whereas the image of the TiO_2 displayed that the TiO_2 particles are microsphere particles. According to the results obtained, the dispersion of the particles has shown to be well dispersed and evenly distributed

throughout the entire layer of coating. Hence, the radiative cooling process can happen efficiently.
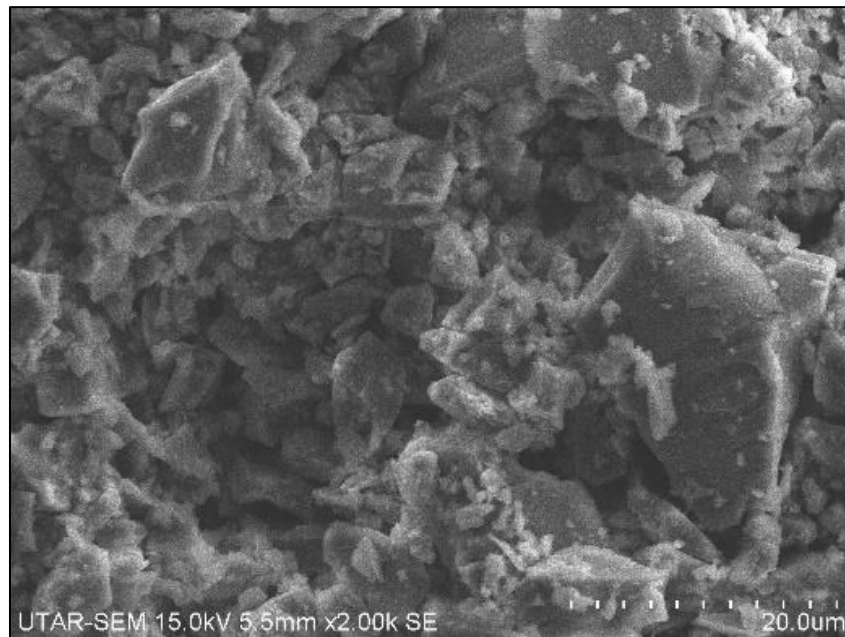
Figure 4.1: SEM image of SiO_2
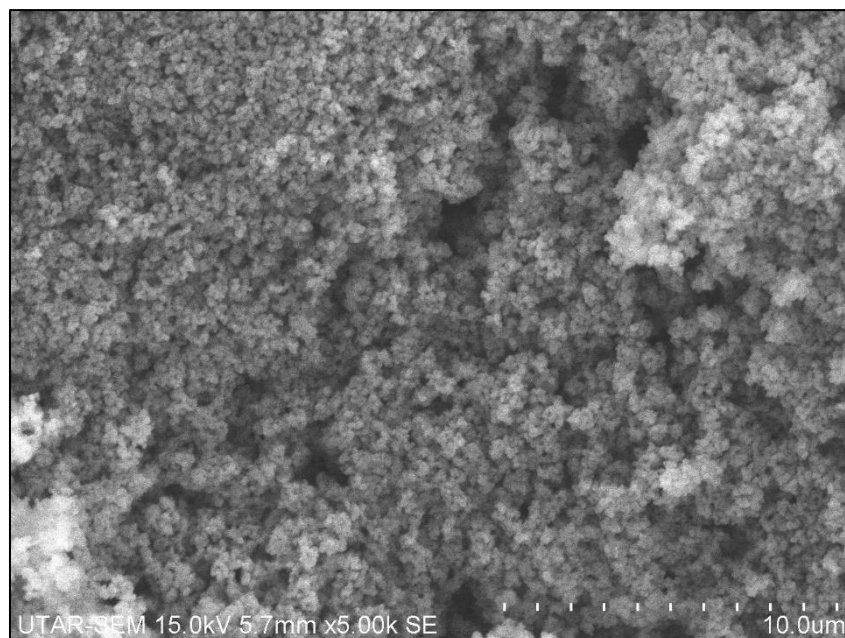
Figure 4.2: SEM image of TiO_2

4.2.2 Energy Dispersive X-ray (EDX)

The samples of SiO_2 and TiO_2 were also followed up with the EDX analysis after the SEM analysis. The data gathered from the EDX machine is displayed in Figure 4.3 for SiO_2 and Figure 4.4 for TiO_2. The primary mineral contents in wt.% were tabulated in Table 4.1: Primary Elemental Composition of SiO_2 and TiO_2. It was found that elements in SiO_2 had Silica (Si) and Oxygen (O) at 54.43 wt.% and 45.57 wt.% respectively. On the other hand, the TiO_2 had elements of Titanium (Ti) and Oxygen (O) at 66.62 wt.% and 33.38 wt.% respectively. These are the primary elemental composition of both materials. The results obtained showed that both materials which are SiO_2 and TiO_2 showed to have contained very minimal to no impurities.

Element	Wt%	At%
OK	45.57	59.51
SiK	54.43	40.49
Matrix	Correction	ZAF
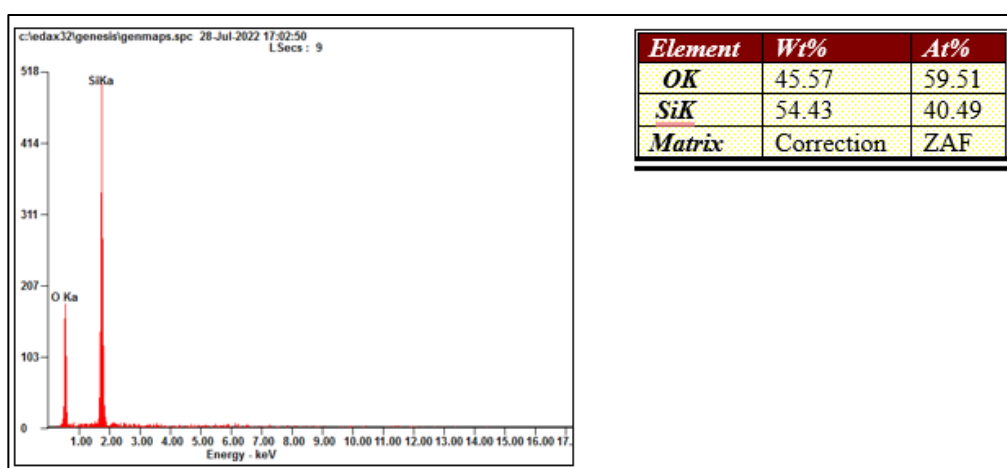
Figure 4.3: EDX Analysis for SiO_2

Element	Wt%	At%
OK	33.38	60.00
TiK	66.62	40.00
Matrix	Correction	ZAF
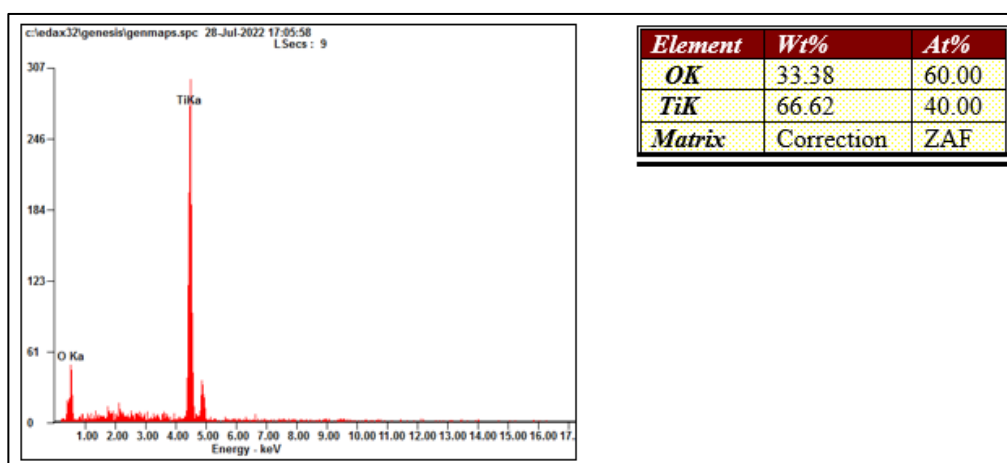
Figure 4.4: EDX Analysis for TiO_2

Table 4.1:   Primary Elemental Composition of SiO_2 and TiO_2

Sample	Element (wt.%)		
	Si	Ti	O
SiO_2	54.43	-	45.57
TiO_2	-	66.62	33.38

4.3   Characterisation of Silicon Dioxide (SiO_2) and Titanium Dioxide (TiO_2) with X-ray Diffraction (XRD)

In this project, four samples were analysed under the XRD machine, the four samples being, SiO_2 coating, SiO_2 powder, TiO_2 coating, and TiO_2 powder. The results were obtained from the XRD machine and plotted in Figure 4.5 for SiO_2 coating, Figure 4.6 for SiO_2 powder, Figure 4.7 for TiO_2 coating and Figure 4.8 for TiO_2 powder.

According to Wonganan et al (2020), silicon dioxide (SiO_2) was detected in peak diffraction of $2\theta \sim 21.5°$, $26.7°$, $43.0°$, and $49.3°$. In Figure 4.5 and Figure 4.6, the results exhibit diffraction peaks at $2\theta \sim 21.5°$, $26.7°$, $43.0°$, and $49.3°$ showing evidence of the presence of SiO_2. The experimental data of the XRD patterns agrees with the JCPDS card no. 21-1272 and other literature sources. The strong diffraction peak at $25°$ shown in Figure 4.7 and Figure 4.8 indicates the TiO_2 anatase structure. Diffraction peaks at $2\theta \sim 25.28°$, $38.08°$, $47.92°$, $53.32°$ and $62.66°$ exhibited the characteristic of TiO_2 for the anatase phase (Kwon et al., 2004). Furthermore, the results shown in Figure 4.7 and Figure 4.8 indicate that the TiO_2 coating and TiO_2 powder do not present any peaks assigned to the rutile phase ($2\theta = 27.36°$).
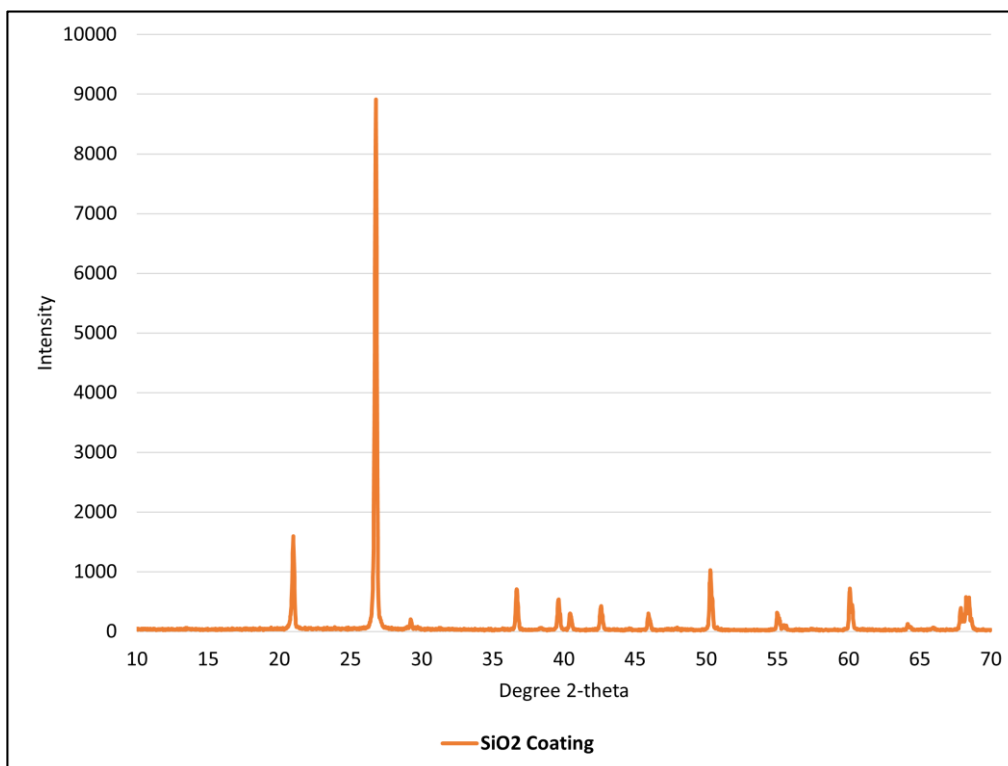
Figure 4.5: X-ray Diffraction pattern for SiO₂ Coating
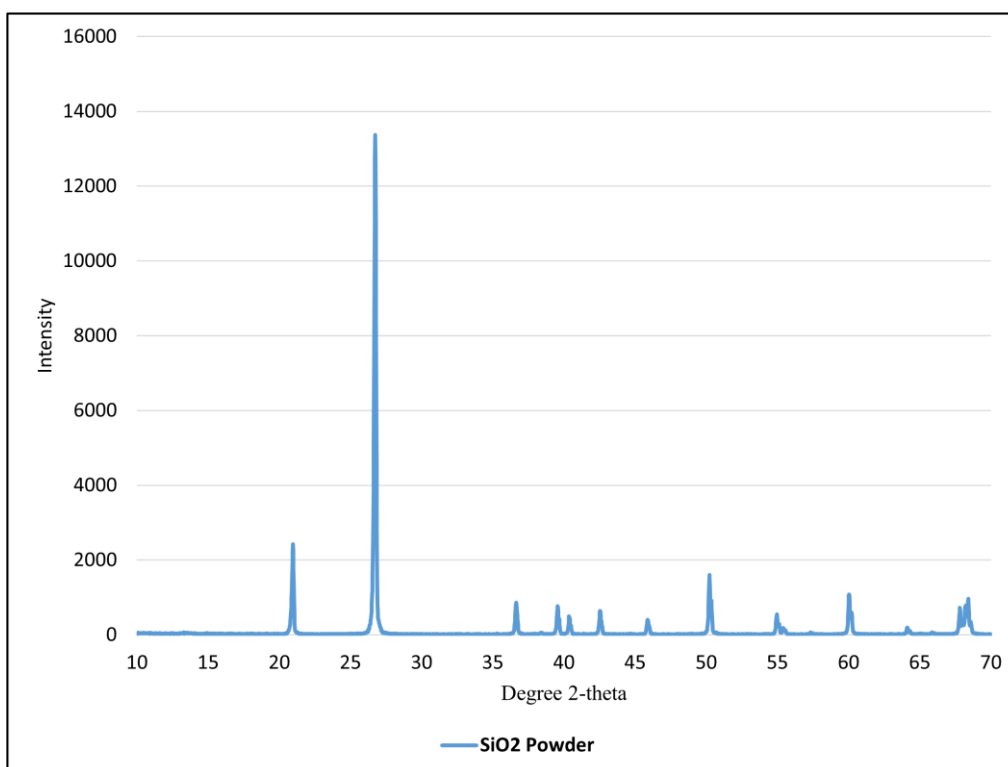
Figure 4.6: X-ray Diffraction pattern for SiO₂ Powder
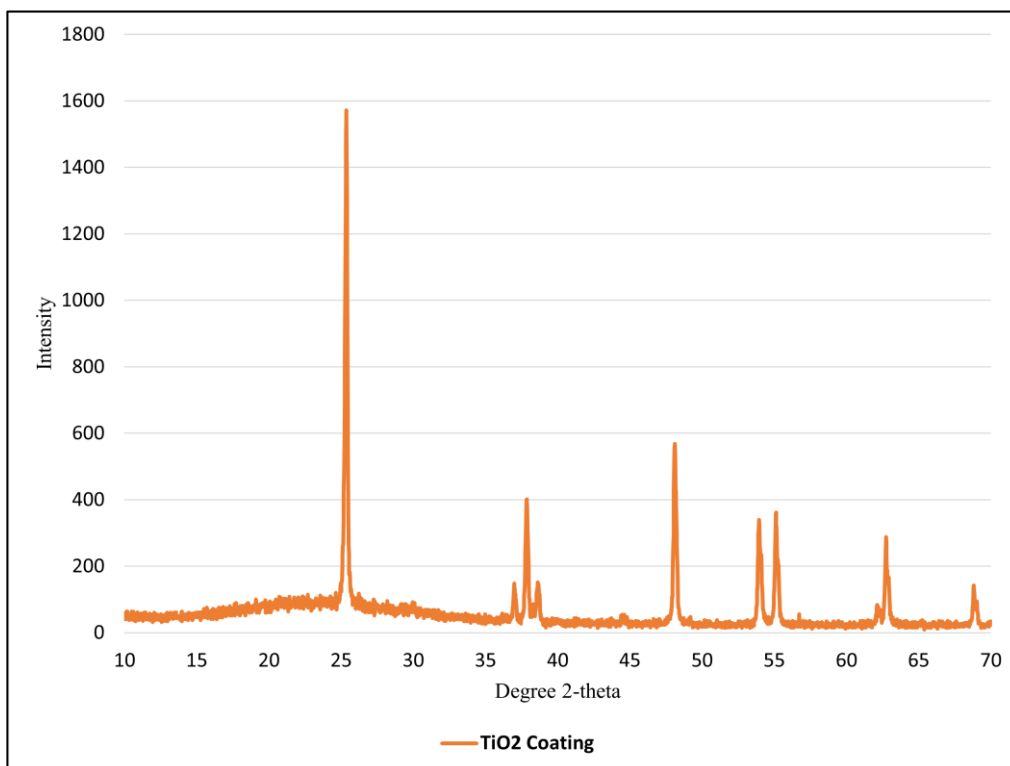
Figure 4.7: X-ray Diffraction pattern for TiO$_2$ Coating
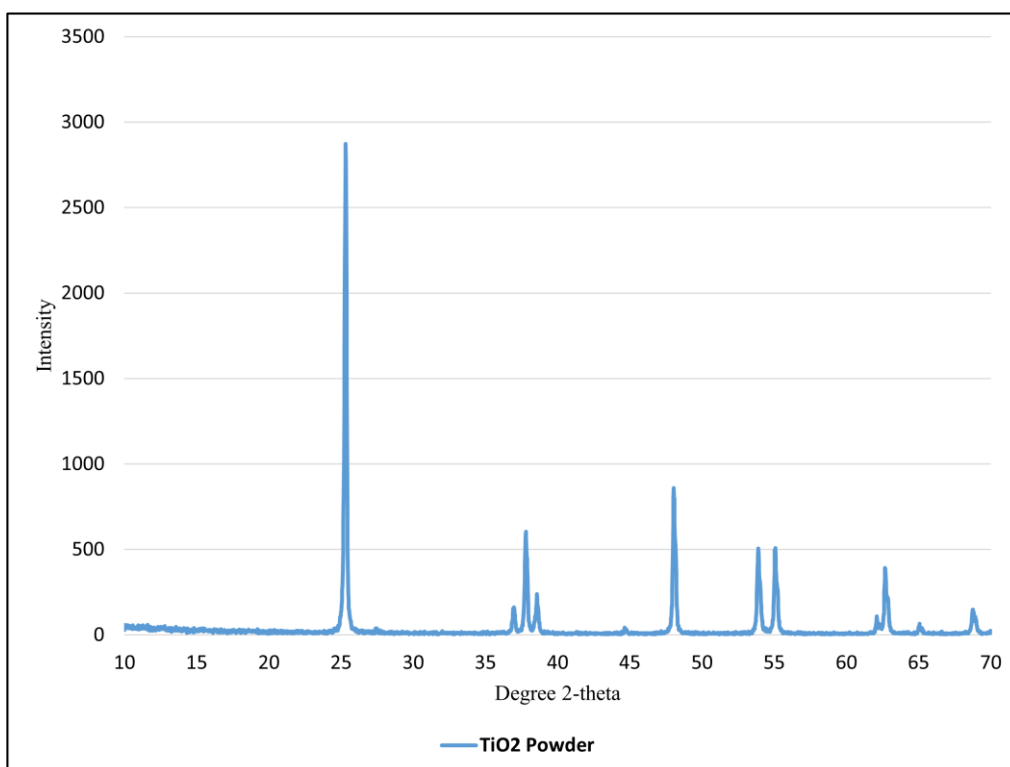
Figure 4.8: X-ray Diffraction pattern for TiO$_2$ Powder

4.4 Prototype with Single-layer Silicon Dioxide (SiO₂) Radiative Cooling Coating (Prototype A)

In this single-layered radiative cooling coating, the material of choice was silicon dioxide (SiO_2). According to Mohammed et al. (2020), SiO_2 is a material that is inorganic, optically transparent, has a low refractive index, and within the atmospheric window of infrared radiation it has high absorption and emission. The purpose was to observe how the SiO2 coating cools down the surface of the TEG modules and how much voltage can be generated with the help of the cooling effect contributed by the SiO_2 coating. During the period of the experiment, a thermal imaging camera was used to take a picture of the surface of the radiative cooling coating which is shown in Figure 4.9. The image displayed that the temperature of the SiO_2 radiative cooling coating showed to have a slightly lower temperature as compared to the surroundings.
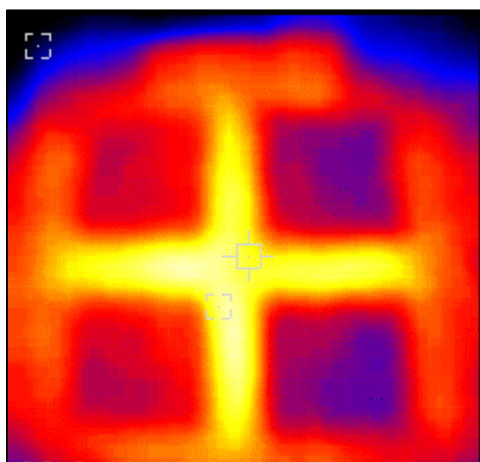
Figure 4.9: Thermal image of SiO_2 coating

There are a few parameters that were recorded, the results in terms of the temperature of the hot and cold sides were plotted in Figure 4.10. The hot side refers to the aluminium heatsinks, and the cold side refers to the surface of the SiO_2 coating on the TEG modules. From Figure 4.10, the hot side temperature displayed a higher temperature reading than the cold side throughout the experiment as the aluminium heatsinks act as a heat reservoir for the prototype. During the time of the experiment, the highest temperature recorded for the hot side and cold side were 52.2 °C and 50.4 °C respectively which took place at 4 pm. The lowest temperature recorded for the hot side was

24.8 °C at 4 am and for the cold side was 24.3 °C at 6 am. In this design for the radiative cooling coating, the SiO_2 coating was able to cool the surface of the TEG modules but not for a significantly large amount.
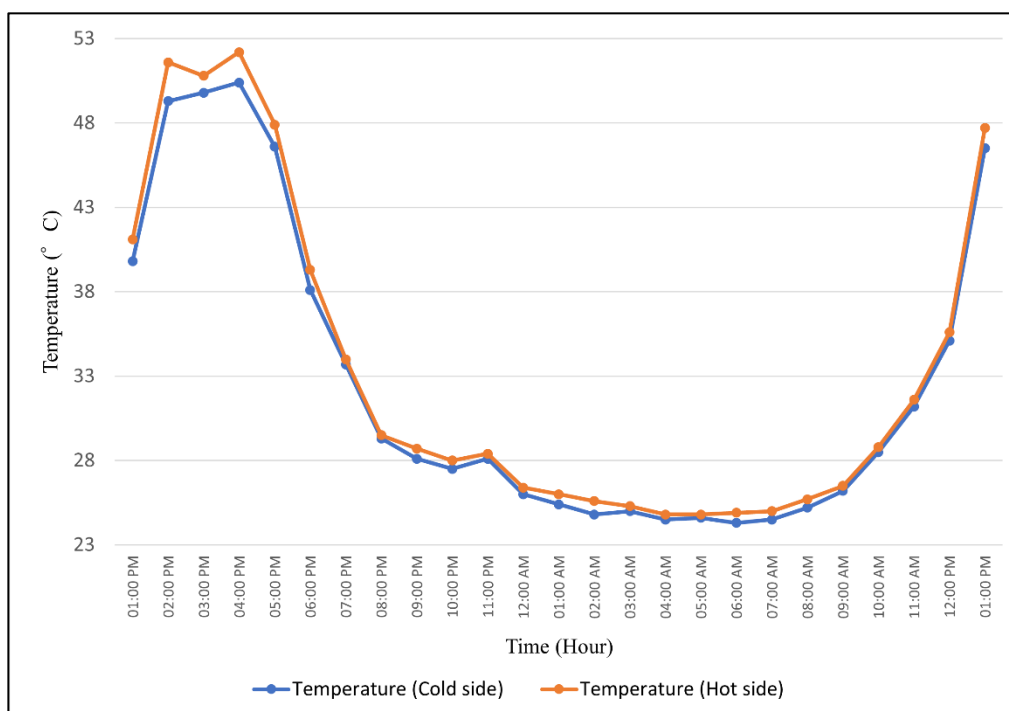
Figure 4.10:   Graph of Temperature against Time (SiO_2)

To successfully generated voltage through the TEG modules, a difference in temperature between the hot and cold sides of the TEG modules had to be present. The recorded results for the temperature difference between the hot and cold sides of the TEG modules were plotted in Figure 4.11. The results fluctuated throughout the period of the experiment. During 2 pm it was recorded to have had the largest temperature difference which was 2.3 °C. During the night-time period, which was between 7 pm to 6 am the results fluctuated between 0.2 °C to 0.8 °C. The average temperature difference for this prototype was 0.71 °C.
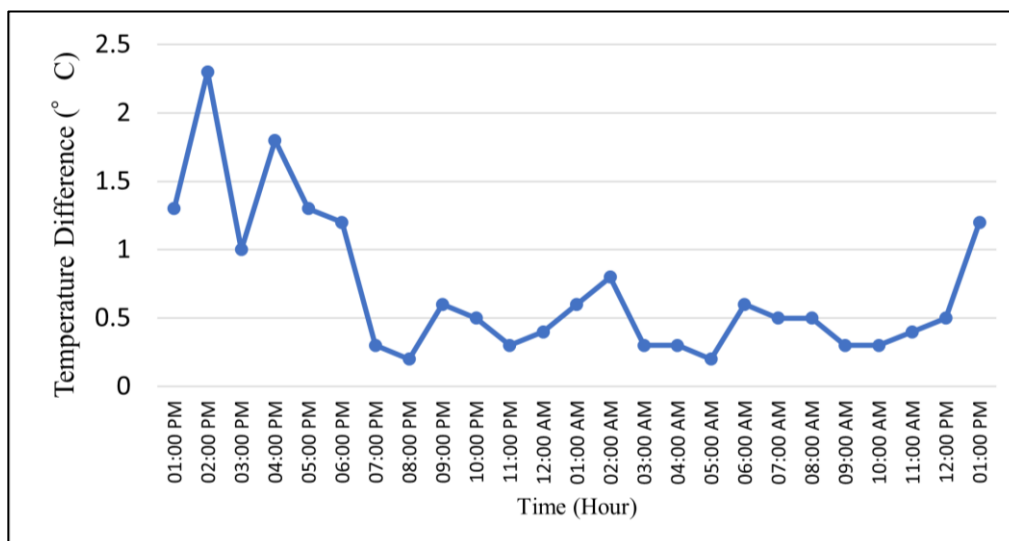
Figure 4.11:   Graph of Temperature Difference against Time (SiO$_2$)

In this experiment, the voltage was successfully generated through the TEG modules which had SiO$_2$ coating on them and the results were plotted in Figure 4.12. At the start of the experiment which was at 1 pm, the voltage generated was fairly low recorded to be 27.6 mV. However, during the afternoon period, the amount of voltage generated started to increase significantly. At 4 pm, the TEG modules had generated 48.9 mV which was the highest throughout the period of the experiment. As time passes, the ambient temperature drops which affect the temperature of both the hot and cold sides thus, the voltage generated also drops to about 10 mV at 7 pm and fluctuates between 4.1 mV to 12.7 mV until 12 pm. The voltage generated between 11 am to 1 pm begun to increase gradually as the ambient temperature increases.
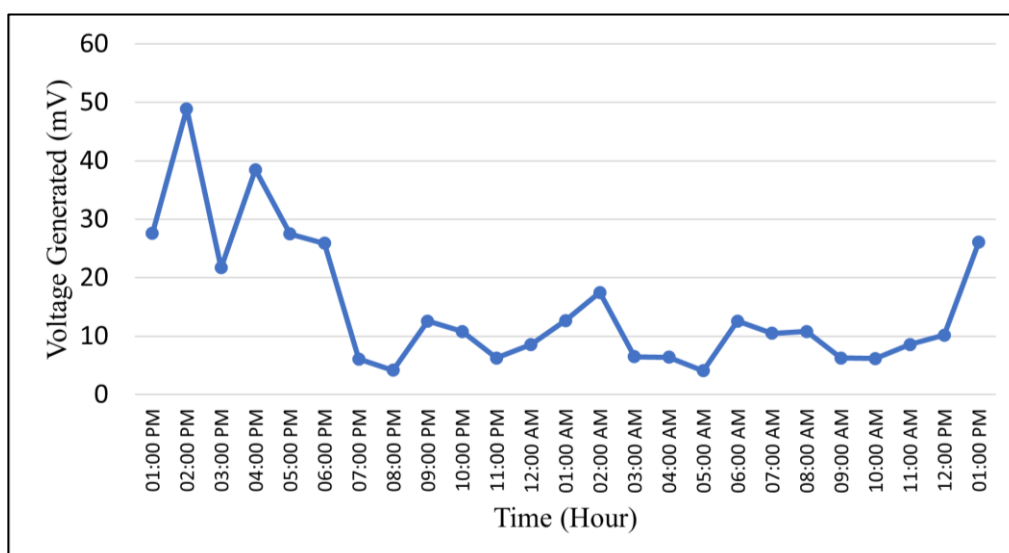
Figure 4.12:   Graph of Voltage Generated against Time (SiO₂)

4.5   Prototype with Single-layer Titanium Dioxide (TiO₂) Radiative Cooling Coating (Prototype B)

In this single-layered radiative cooling coating, the material of choice is titanium dioxide (TiO₂). The purpose of it was to observe how the TiO₂ coating cools down the surface of the TEG modules and how much voltage can be generated with the help of the cooling effect contributed by the TiO₂ coating. In this experiment, the temperature of the hot and cold sides, and the voltage generated were the parameters recorded. Moreover, a thermal imaging camera was used to take an image of the surface of the TiO₂ radiative cooling coating, and the result was displayed in Figure 4.13. It showed that the TiO₂ radiative cooling coating exhibits a lower temperature as compared to its surroundings. TiO₂ is one of the materials used in paints and also serves a function for radiative cooling, it is better to use a highly reflective paint hence, the absorptivity of the pigments must be high (Family & Mengüç, 2017).
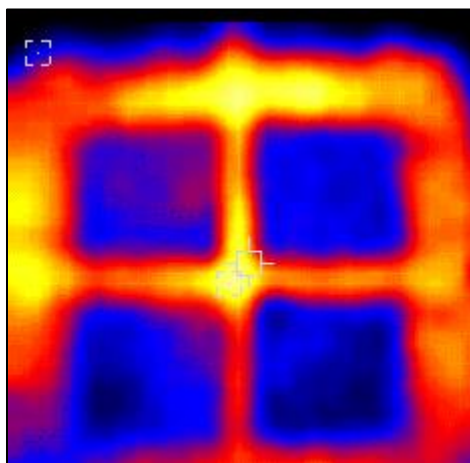
Figure 4.13:   Thermal image of TiO$_2$ coating

The temperature values of the hot and cold sides were shown in Figure 4.14. The temperature of the hot side is almost similar to the temperature of the hot side of the prototype with the SiO$_2$ coating as both prototypes had their results recorded on the same day. Based on Figure 4.15, the temperature of the hot side was always higher than that of the cold side. The highest temperature on the hot side reached 52.4 °C at 4 pm and the lowest temperature reached 24.9 °C at 6 am. On the other hand, the highest temperature on the cold side reached 49.5 °C at 3 pm and the lowest temperature reached 24.5 at 6 am. During the night-time, the TiO$_2$ coating displayed to have lower temperature readings as compared to the hot side of the prototype which is shown in Figure 4.14. For this prototype, the TiO$_2$ coating managed to reduce the temperature of the surface.
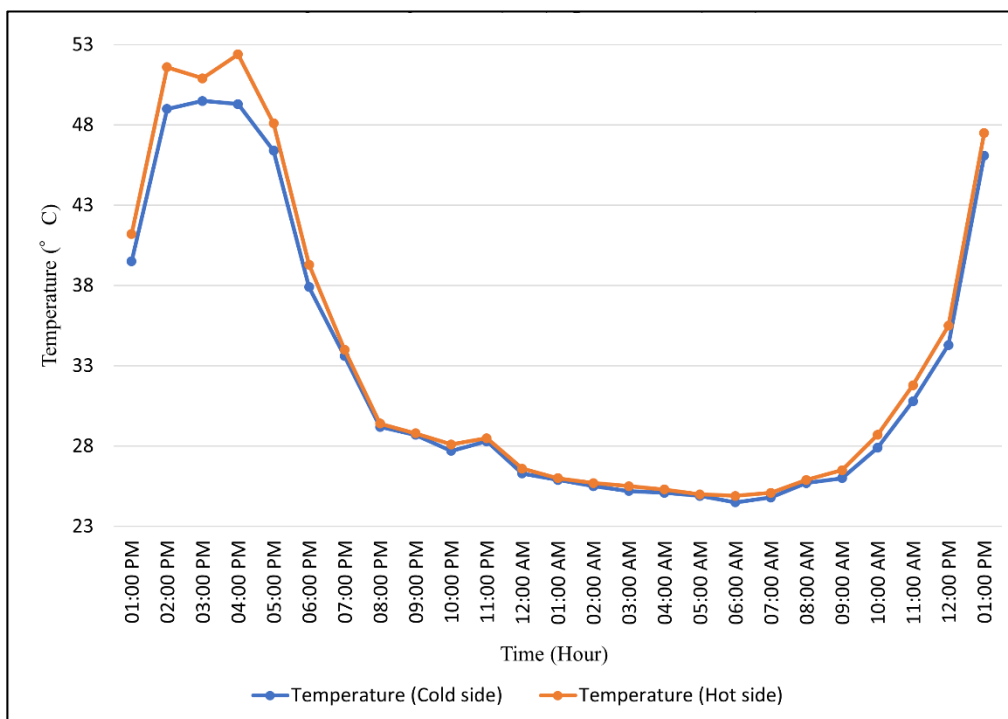
Figure 4.14:   Graph of Temperature against Time (TiO$_2$)
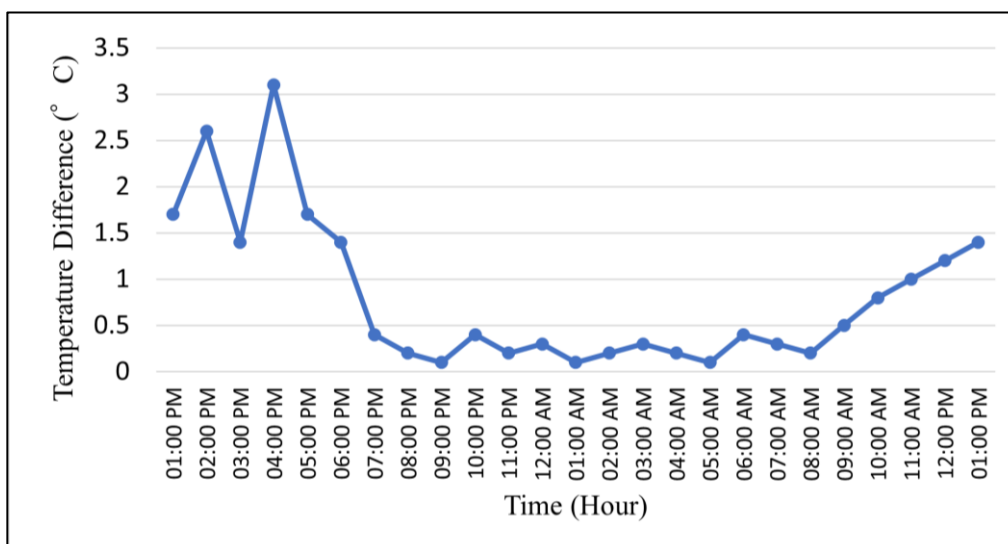
Figure 4.15:   Graph of Temperature Difference against Time (TiO$_2$)

Furthermore, there is the presence of temperature difference across the hot and cold sides of the TEG modules, hence voltage was generated by the prototype throughout the experiment. The results of the temperature difference between the hot and cold sides were plotted in Figure 4.15. The aluminium heatsinks were the hot side and the cold side refers to the surface of the radiative cooling coating. Whereas the results for the voltage generated were plotted in

Figure 4.16. During the afternoon period which is from 1 pm to 5 pm, there was a fluctuation in the temperature difference which is shown in Figure 4.15. However, at 2 pm, the highest reading for the temperature difference was 3.1 °C. And after sunset, which started at 8 pm, the temperature difference readings fluctuated between 0.1 °C to 0.4 °C. The average temperature difference for this prototype was 0.81 °C.

Moreover, with the difference in temperature, prototype B was able to generate voltage and the results were plotted in Figure 4.16. Throughout the 24 hours, the highest voltage reading generated was at 66.4 mV which took place at 4 pm. The lowest voltage reading generated was 2.2 mV at the time of 1 am. In the period of 7 pm to 8 am, based on Figure 4.16, the voltage generated was constantly below 10 mV. As the sun rises and the surrounding temperature started to rise as well, the temperature difference between the hot and cold sides increased gradually and thus the voltage generated by the prototype also increased gradually, which was displayed in Figure 4.16, between the period of 8 am to 1 pm.
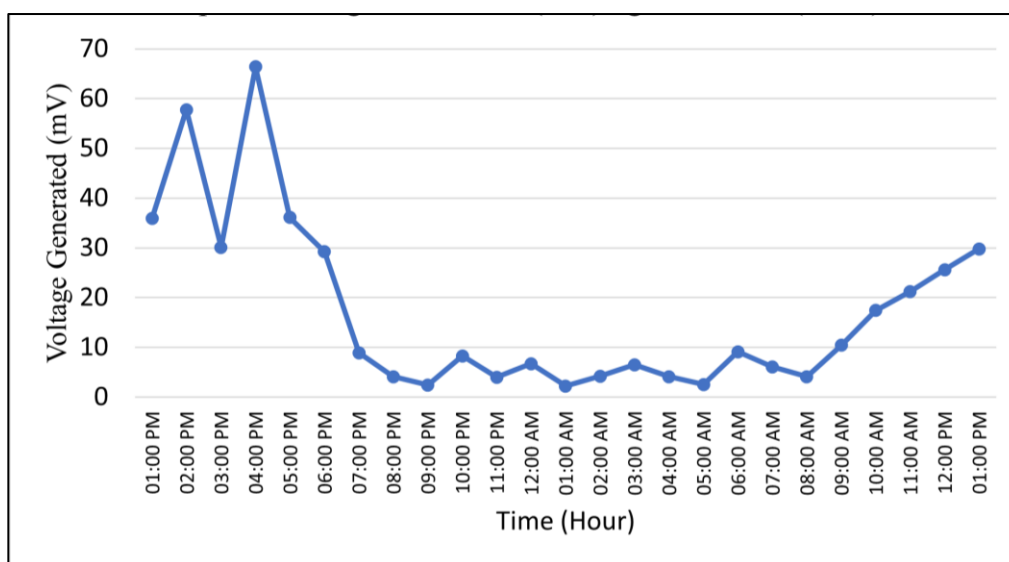
Figure 4.16: Graph of Voltage Generated against Time (TiO_2)

4.6 Prototype with Double-layer (SiO_2+TiO_2) Radiative Cooling Coating (Prototype C)

In this double-layered radiative cooling coating, the two layers consist of different materials and the materials of choice were silicon dioxide (SiO_2) as the

bottom layer and titanium dioxide (TiO$_2$) as the top layer. During the period of the experiment, a thermal imaging camera was used to take a picture of the surface of the TEG modules that were coated with the double-layered coating and the result was displayed in Figure 4.17. The results indicate that the 4 surfaces of the TEG modules displayed a lower temperature than the surrounding which means that the double-layered radiative cooling coating has a significant cooling effect. The purpose of this double-layered radiative cooling coating and the choices of materials was to observe how the coating cools down the surface of the TEG modules and how much voltage can be generated by the prototype with the help of the cooling effect contributed by the radiative cooling coating. In this experiment, parameters that were measured were the temperature of the hot and cold sides of the TEG modules and the voltage generated by the prototype.
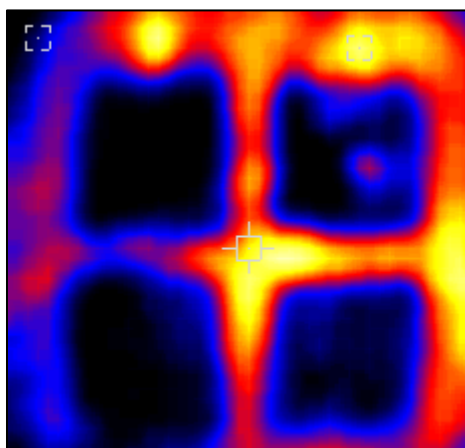
Figure 4.17:   Thermal image of SiO$_2$+TiO$_2$ coating

Firstly, the temperature readings of the hot and cold sides of the prototype were recorded and plotted in Figure 4.18. The hot side refers to the aluminium heatsinks, and the cold side refers to the surface of the radiative cooling coating. Based on the graph in Figure 4.18, the temperature of the cold side is significantly lower than the temperature of the hot side. Overall, the temperature of both sides rises during the afternoon period and gradually decreases as the sun sets and the ambient temperature decreases. The highest temperature recorded for the hot side was 59 °C and for the cold side was 56.2 °C which both happened at 2 pm. On the contrary, the lowest temperature

reached on the hot side was 25.7 °C at 6 am and on the cold side was 24.7 °C at 5 am. The temperature gradually decreases as time passes by and decreases more after the sunset which also causes the ambient to decrease.
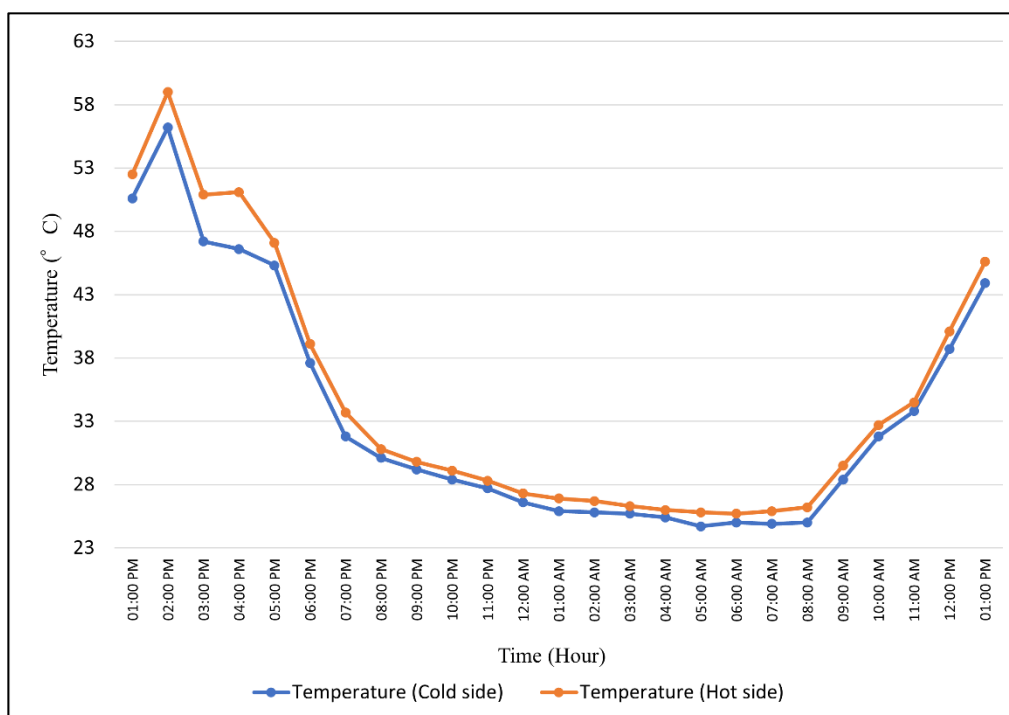
Figure 4.18:   Graph of Temperature against Time (SiO$_2$+TiO$_2$)

Based on the temperature readings of the hot and cold sides recorded, the results of the temperature difference between both sides were plotted in Figure 4.19. During the afternoon period between 1 pm to 4 pm, the temperature difference increased gradually and decreases sharply afterwards. The largest value of temperature difference recorded was 4.5 °C at 4 pm. Furthermore, from 8 pm to 11 am the temperature differences were always above 0.5 °C. After 11 am, the temperature difference increased again as was due to the increase in surrounding temperature and the cooling effect of the radiative cooling coating. Furthermore, the average temperature difference for this prototype was 1.7 °C.

On the other hand, prototype C successfully generated voltage throughout the period of the experiment and the results were plotted in Figure 4.20. In terms of voltage generated, this prototype generated the highest value of the voltage of 96.5 mV at 4 pm. The voltage generated gradually increased from 1 pm to 4 pm and then decreases gradually after 4 pm until 8 pm. From 8

pm until 11 am, the voltage generated fluctuated between 12.6 mV to 25.7 mV. The voltage generated gradually increased from 11 am to 1 pm due to the increase in ambient temperature and the cooling effect of the double-layered radiative cooling coating.
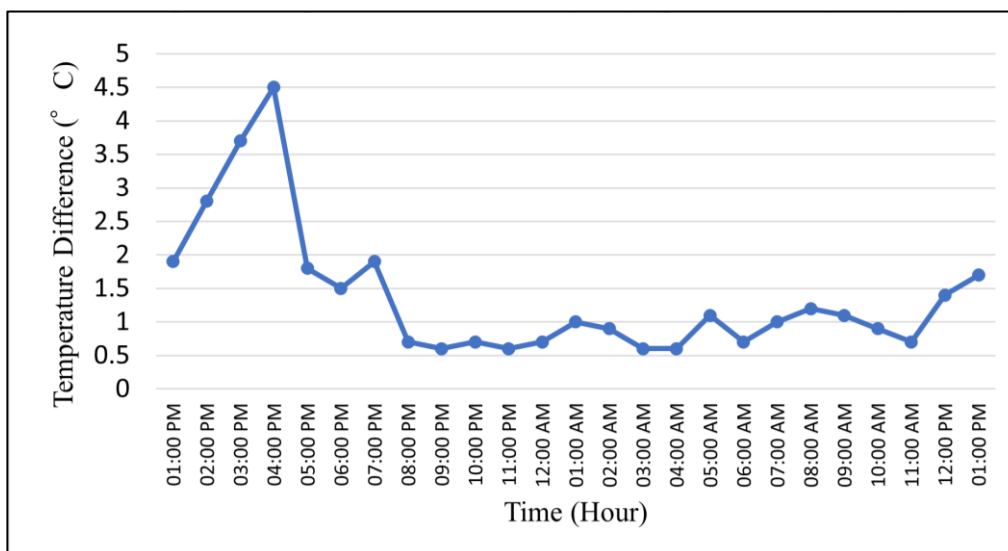
Figure 4.19: Graph of Temperature Difference against Time (SiO_2+TiO_2)
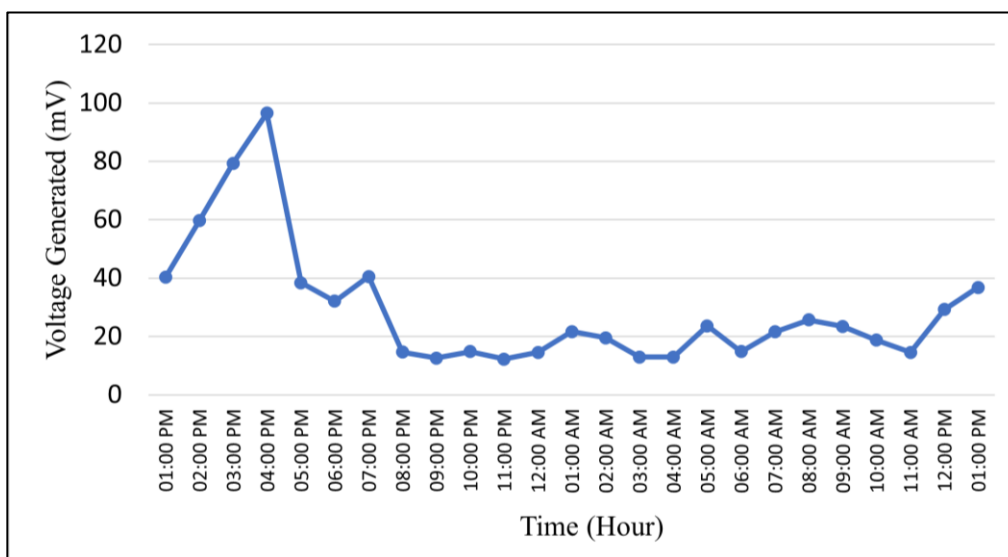
Figure 4.20: Graph of Voltage Generated against Time (SiO_2+TiO_2)

4.7   Comparison of results between prototypes

4.7.1   Comparison between prototype with SiO₂ radiative cooling coating (Prototype A) and prototype with TiO₂ radiative cooling coating (Prototype B)

Based on the results obtained and plotted in Figure 4.21, during the day, the temperature difference between the hot and cold sides of prototype B was higher than that of prototype A. On the contrary, the temperature difference of prototype A was higher than that of prototype B during the night. Furthermore, both prototypes had almost similar temperatures on the hot side which can be considered constant.
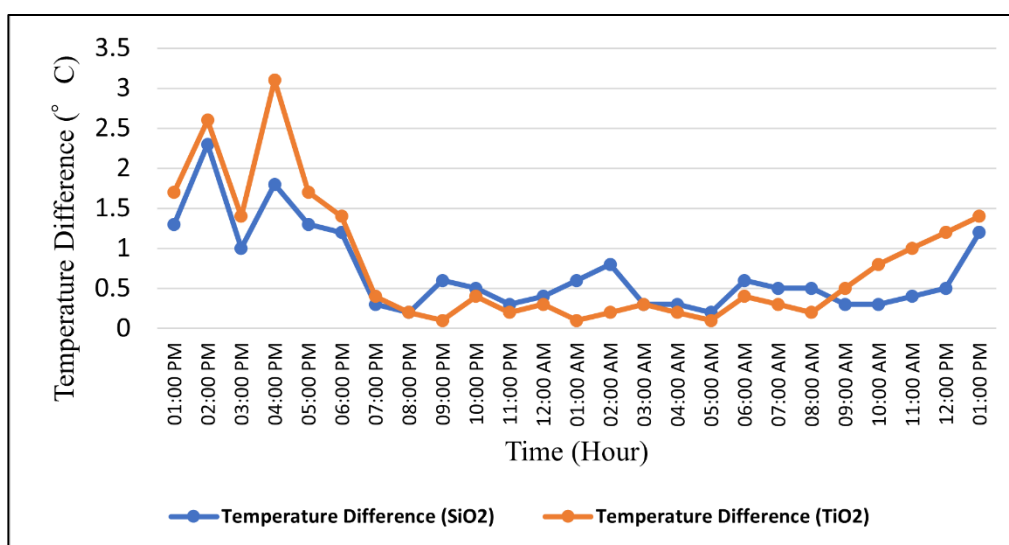
Figure 4.21:   Graph of Temperature Difference against Time (Comparison SiO₂ and TiO₂)

Temperature and temperature difference are one of the few crucial parameters when it comes to TEG applications, when the temperature difference increases, the power output also increases (Pourkiaei et al., 2019). Based on that literature, it justifies the results shown in Figure 4.22, that is during the day, the voltage generated by prototype B was higher than the voltage generated by prototype A. On the other hand, the voltage generated by prototype A was higher than the voltage generated by prototype B during the night. The Seebeck effect takes place when there is a temperature difference that conclusively generates a

voltage (Jouhara et al., 2021). TiO$_2$ particles are considered efficient solar reflectors due to their ability to strongly scatter sunlight (Bao et al., 2017).
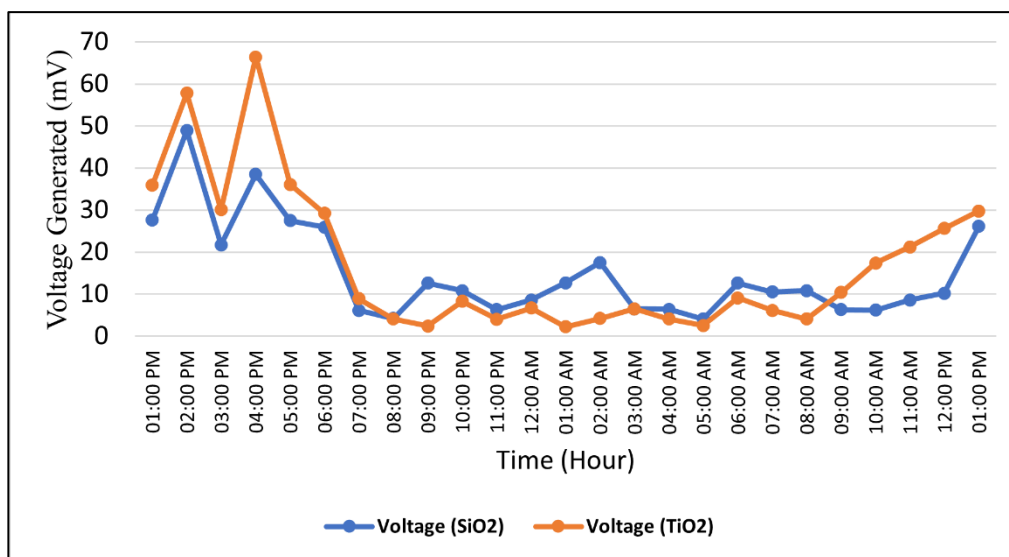
Figure 4.22:   Graph of Voltage Generated against Time (Comparison SiO$_2$ and TiO$_2$)

As there was a difference in temperature between the hot and cold sides for all three prototypes, hence the Seebeck effect took place and the TEG modules produced voltage in the end. However, even though being able to utilize the Seebeck effect to generate voltage, the performance of the radiative cooling coating could also be affected by various factors. One of the factors is relative humidity, as it influences the spectral transmittance thus affecting the radiative cooling performance (Bao et al., 2017). Throughout the experiment, the skies were partly cloudy which also affects the radiative cooling performance. The conditions of the skies in the afternoon during the time of the experiment are shown in Figure 4.23.

Figure 4.23:   Condition of skies (partly cloudy)

4.7.2   Comparison between prototype with SiO$_2$+TiO$_2$ radiative cooling coating (Prototype C) and both prototypes with single-layer SiO$_2$ and TiO$_2$ radiative cooling coating (Prototype A and B)

The double-layered radiative cooling coating consisted of SiO$_2$ coating as the bottom layer and TiO$_2$ coating as the top layer. The temperature difference between the hot and cold sides of prototype C had shown to be greater than that of prototypes A and B and is shown in Figure 4.24. Thus, Figure 4.25 exhibited that prototype C generated more voltage as compared to both prototypes A and B. Based on the research conducted by Bao et al. (2017), a coating made with SiO$_2$ + TiO$_2$ can achieve lower temperature as it has the selective emissivity peak in the "sky window" and according to their research, the surface that had the TiO$_2$ + SiO$_2$ coating achieved the lowest stagnation temperature that was approximately 5°C lower than ambient temperature. Both TiO$_2$ and SiO$_2$ can provide highly selective thermal radiation within the transparent window and the reason for that is because, in the 8-13 μm wavelength range, both materials have a high value of imaginary permittivity (Jeong et al., 2020).
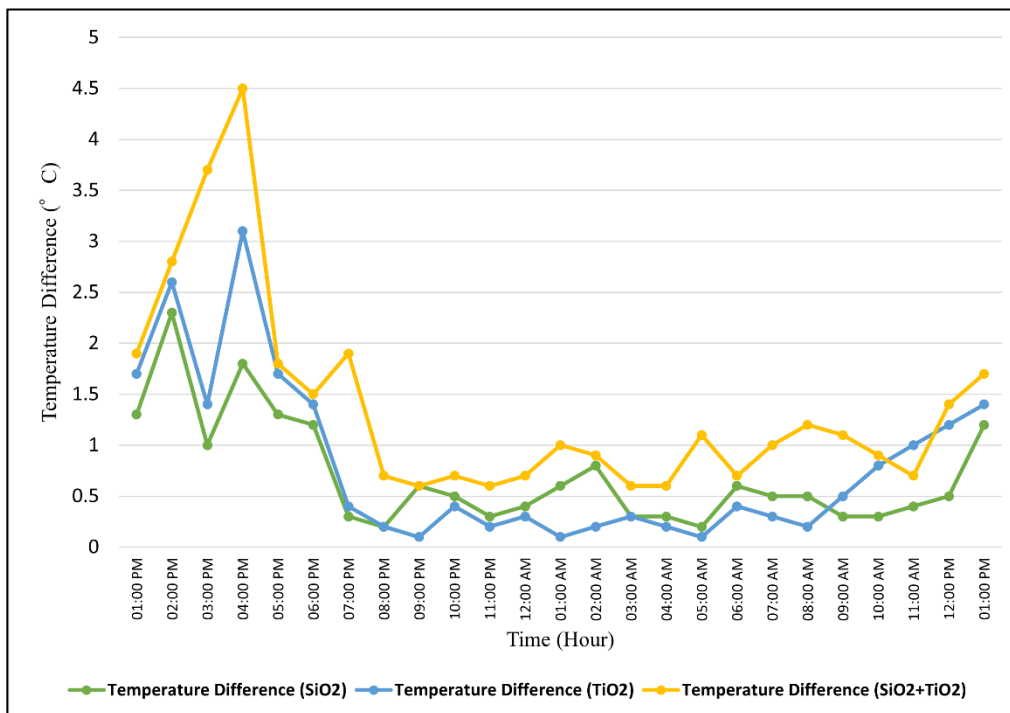
Figure 4.24:   Graph of Temperature Difference against Time (All three prototypes)
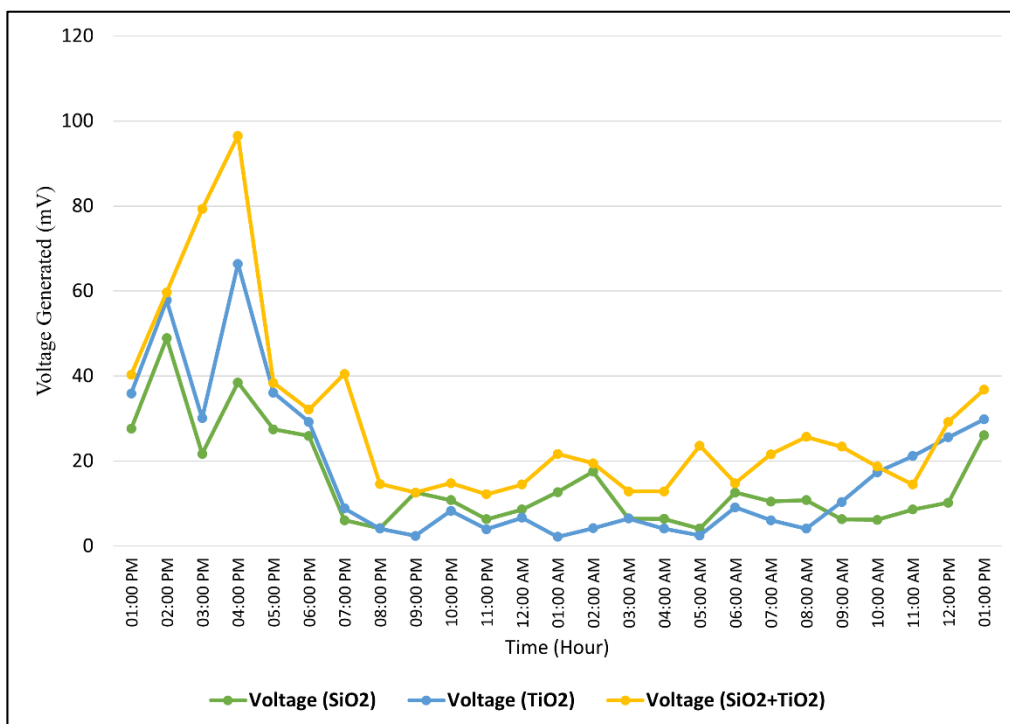
Figure 4.25:   Graph of Voltage Generated against Time (All three prototypes)

The double-layered radiative cooling coating exhibited to have performed better than both single-layered radiative cooling coating in terms of voltage generated and the temperature difference across the hot and cold sides of the prototype. The average voltage generated by prototype C was 29.2 mV whereas for prototype A it was 15 mV and for prototype B it was 17.3 mV. On the other hand, in terms of temperature difference, prototype C managed to achieve an average temperature difference of 1.4 °C whereas prototype A achieved an average temperature difference of 0.71 °C and prototype B achieved an average temperature difference of 0.81 °C. To justify that, SiO_2 coating works as a selective emitter and the TiO_2 coating serves as a solar reflector. There are various atmospheric conditions across different locations, thus, to implement radiative cooling in practice, more than 94% of the sunlight must be reflected to achieve meaningful daytime radiative cooling (Raman et al., 2014). Not to mention that, for prototype C, the average temperature difference is 1.4 °C which is almost twice as much as that of both the single-layered radiative cooling coating prototypes.

4.8   Efficiency and Output Power of each prototype

According to Harun et al. (2018), the thermal conductivity for the TEG module (TEC1-12706) is k = 1.5 $Wm^{-1}K^{-1}$ and the thermal resistivity based on the data sheets is 1.98 Ω, also, T_H = 131 °C and T_L = 33 °C. Therefore, the maximum efficiency of the TEG modules is calculated using Equation (3.3). The results were tabulated and shown in Table 4.2.

Table 4.2:   Seebeck Coefficient and Efficiency of Prototypes

Prototype	Seebeck Coefficient (mV/°C)	Efficiency, N (%)
A	21.312	0.3716
B	21.441	0.3761
C	21.306	0.3715

Based on the results obtained throughout the period of the experiment, the results were used to calculate the power generated by each prototype using

Equation 3.6. The power generated by each prototype was shown in Figure 4.26 for prototype A, Figure 4.27 for prototype B and Figure 4.28 for prototype C. The average power generated was also calculated and the average power generated for prototype A, prototype B and prototype C were 0.178 mW, 0.3 mW and 0.655 mW respectively. In research conducted by Byon and Jeong (2020), their design was also based on a passive electricity generator concept that uses a thermoelectric generator, their source of heat was building walls and there were 4 TEG modules used and the results showed that the design had an average electric power of 0.01 W and the largest temperature difference obtained was 32 °C. In another study conducted by Gou et al. (2010), the concept implemented was using the thermoelectric generator for low-temperature waste heat recovery, they used ten pieces of TEG modules and implemented hot water as the heat source. Based on the results obtained from their experiment, the maximum output power was found to be 0.85 W with a maximum temperature difference of 58 °C.
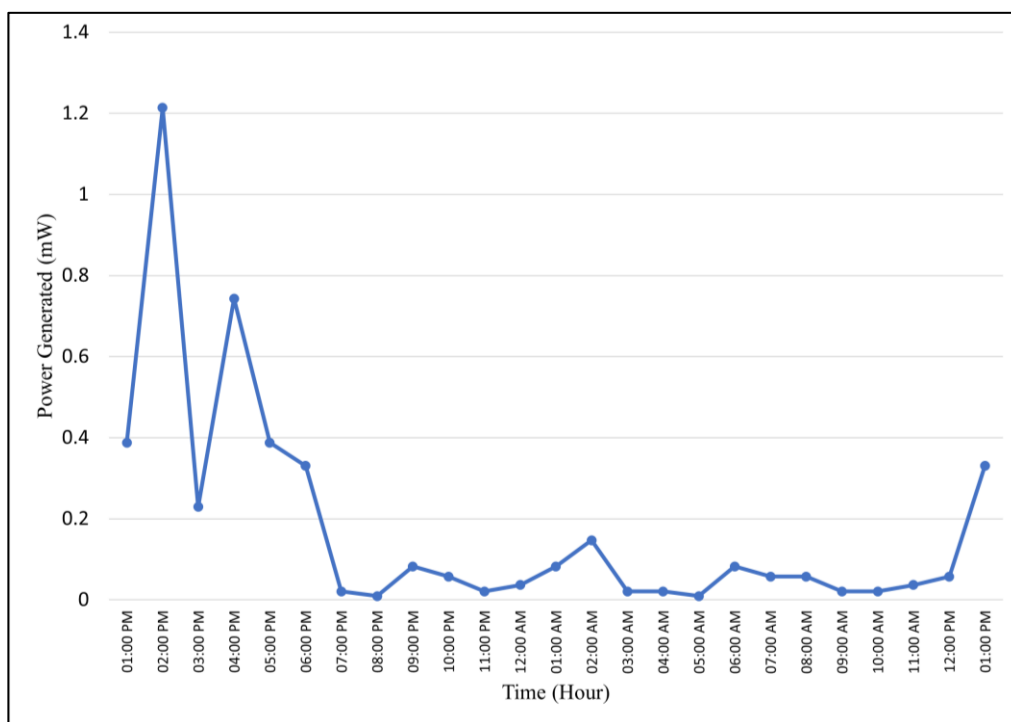
Figure 4.26:   Graph of Power Generated (Prototype A)

61
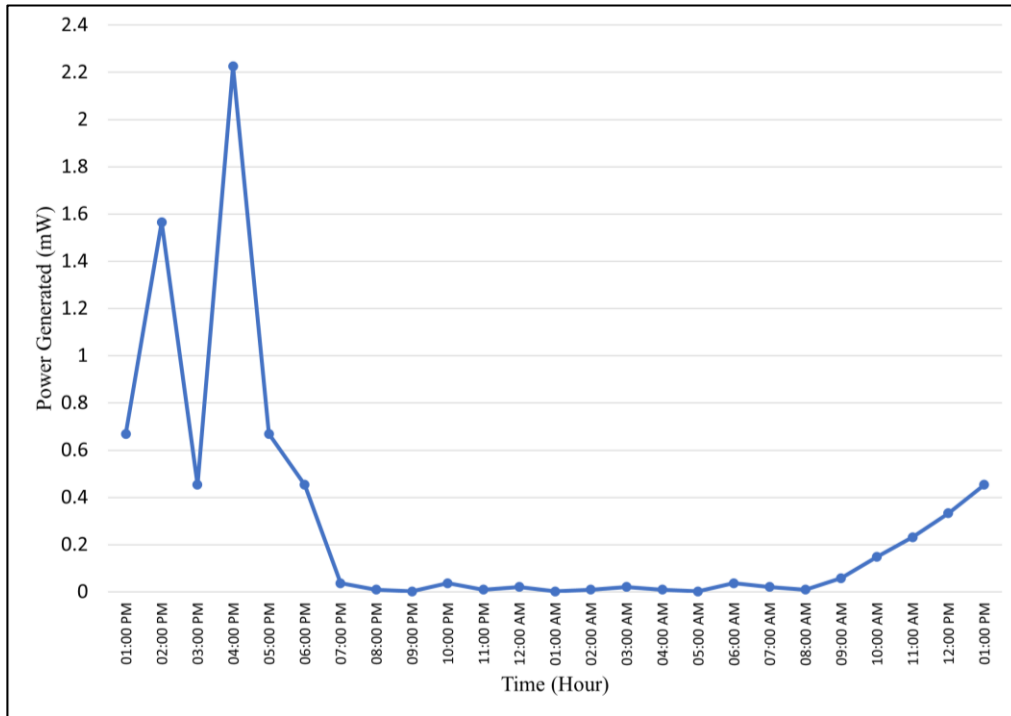
Figure 4.27:   Graph of Power Generated (Prototype B)
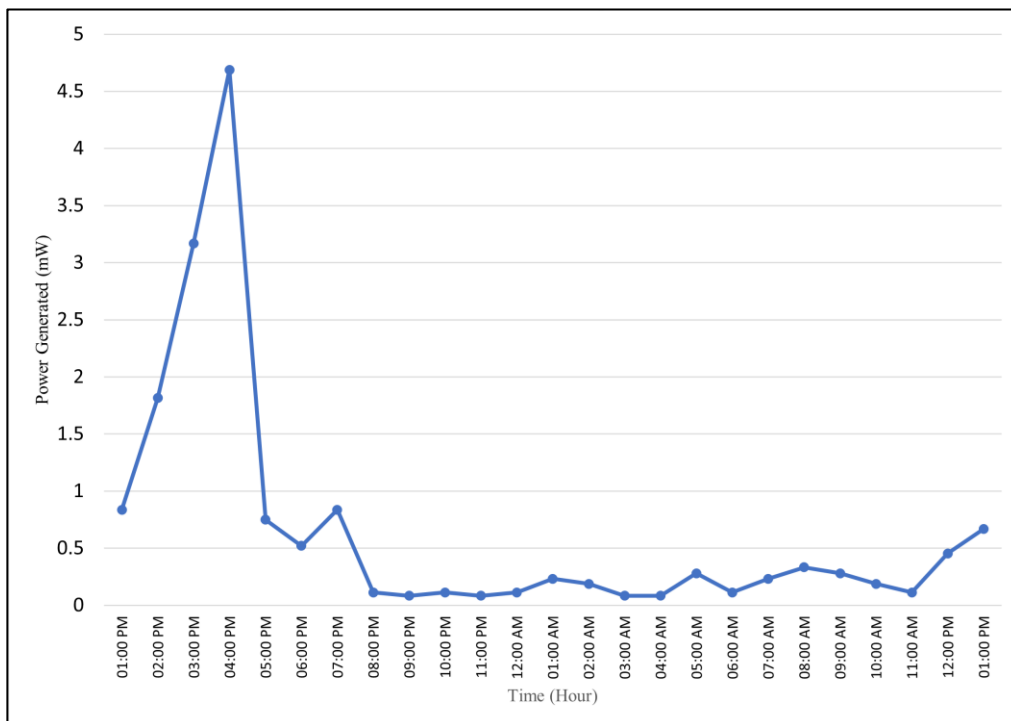
Figure 4.28:   Graph of Power Generated (Prototype C)

CHAPTER 5

CONCLUSION AND RECOMMENDATIONS

5.1   Conclusion

In conclusion, the application of radiative cooling with thermoelectric for power generation had been proven in this project. Prototype models for radiative cooling-thermoelectric generator were successfully developed and proved to have generated power. Both SiO_2 and TiO_2 had showed different cooling effects and the performance of each prototype model were evaluated and compared. Furthermore, prototype C showed to have performed the best among all the prototypes in terms of temperature difference generated and voltage generated, and power generated. However, all radiative cooling coating in this experiment exhibited cooling effects based on the thermal image taken and the results obtained. Both SiO_2 and TiO_2 had proven to be suitable for radiative cooling applications but when used together both of them can generate a better result as compared to when using them individually. Based on the experiment conducted, the average temperature difference generated by each prototype was 0.71 °C for prototype A, 0.81 °C for prototype B and 1.4 °C for prototype C. To justify the results obtained, prototype C managed to generate an overall higher amount of voltage throughout the experiment with a peak voltage of 96.5 mV. Not to mention that the average power generated by prototype C was 0.655 mW was also the highest among the three prototypes.

The materials were analysed using SEM-EDX and XRD before the experiment to study their characteristics. Moreover, the bar coating method was an efficient and reliable method to layer coatings onto substrates, in this project, all coatings were coated evenly, and no impurities were found on the coatings. Not to mention there are several factors that could affect the efficiency of radiative cooling. One of the major factors is the weather, radiative cooling efficiency is decreased when there is the presence of many clouds and rain. The optimal situation where radiative cooling can happen would be when there are clear skies with no clouds and the relative humidity of the surroundings is low.

5.2 Recommendation

There are several methods and recommendations that can be ventured to improve this research project in the future. One of the recommendations would to be undergo the experiment under clear skies with no clouds conditions and when the relative humidity of the surroundings is low. This can further enhance the efficiency of the radiative cooling mechanism. Checking weather forecasts from different platforms or websites is recommended to prevent stopping the experiment halfway if the weather rains or gets too windy.

The optimisation process for SiO_2 and TiO_2 particles is also suggested for future studies. Thus, the most optimal shape and size of the particles as well as the thickness of the coatings can be determined which ultimately leads to a better radiative cooling process and the results generated can be improved.

There are also several types of coating that can be used for the application of radiative cooling coating. For instance, polymeric coating and coatings with nanophotonic structures can be explored. Each type of coating exhibits different results and unique benefits.

Lastly, the use of sputtering deposition methods is recommended for future studies. By using this method, there are several parameters of the coating that can be controlled well. For example, the deposition rate, uniformity, composition, and thickness control. Furthermore, with the sputtering deposition method, the coating for radiative cooling can be created more efficiently and precisely.

REFERENCES

Assawaworrarit, S., Omair, Z. & Fan, S., 2022. Nighttime electric power generation at a density of 50 MW/m2 via radiative cooling of a photovoltaic cell. *Applied Physics Letters*, 120(14), p.143901.

Bao, H., Yan, C., Wang, B., Fang, X., Zhao, C. and Ruan, X., 2017. Double-layer nanoparticle-based coatings for efficient terrestrial radiative cooling. *Solar Energy Materials and Solar Cells*, 168, pp.78-84.

Byon, Y. and Jeong, J., 2020. Annual energy harvesting performance of a phase change material-integrated thermoelectric power generation block in building walls. *Energy and Buildings*, 228, p.110470.

Chen, M. et al., 2021. Passive daytime radiative cooling: Fundamentals, material designs, and applications. *EcoMat*, 4(1).

Chen, X. et al., 2021. Cellulose-based porous polymer film with auto-deposited TIO2 as spectrally selective materials for passive daytime radiative cooling. *Optical Materials*, 120, p.111431.

Cheng, Z.M. et al., 2020. Optical properties and cooling performance analyses of single-layer radiative cooling coating with mixture of tio2 particles and SIO2 particles. *Science China Technological Sciences*, 64(5), pp.1017–1029.

Fu, Y. et al., 2022. Polymer coating with gradient-dispersed dielectric nanoparticles for enhanced daytime radiative cooling. *EcoMat*, 4(2).

Gou, X., Xiao, H. and Yang, S., 2010. Modeling, experimental study and optimization on low-temperature waste heat thermoelectric generator system. *Applied Energy*, 87(10), pp.3131-3136.

Harun, M., Annuar, K., Halim, M., Hasan, M., Aras, M. and Yaakub, M., 2016. Peltier And Seebeck Efficacy Of Hot And Cold Air System For Portable O-REF

(Oven & Refrigerator) Application. *Proceedings of Mechanical Engineering Research Day 2016*, pp.81-82.

Harun, M., Azmi, M., Aras, M., Azlan, U., Azahar, A., Annuar, K., Halim, M., Yaakub, M. and Abidin, A., 2018. A Study on the Potential of Peltier in Generating Electricity Using Heat Loss at Engine and Exhaust Vehicle. *Journal of Advanced Research in Fluid Mechanics and Thermal Sciences 49*, (1), pp.77-84.

Hossain, M.M. & Gu, M., 2016. Radiative cooling: Principles, progress, and potentials. *Advanced Science*, 3(7), p.1500360.

Ishii, S. et al., 2021. Simultaneous harvesting of radiative cooling and solar heating for transverse thermoelectric generation. *Science and Technology of Advanced Materials*, 22(1), pp.441–448.

Ishii, S., Dao, T.D. & Nagao, T., 2020. Radiative cooling for continuous thermoelectric power generation in day and night. *Applied Physics Letters*, 117(1), p.013901.

Jaramillo-Fernandez, J. et al., 2019. A self-assembled 2D thermofunctional material for radiative cooling. *Small*, 15(52), p.1905290.

Jeong, S.Y. et al., 2020. Field investigation of a photonic multi-layered TIO2 passive radiative cooler in sub-tropical climate. *Renewable Energy*, 146, pp.44–55.

Jouhara, H., Żabnieńska-Góra, A., Khordehgah, N., Doraghi, Q., Ahmad, L., Norman, L., Axcell, B., Wrobel, L. and Dai, S., 2021. Thermoelectric generator (TEG) technologies and applications. *International Journal of Thermofluids*, 9, p.100063.

Kwon, C., Shin, H., Kim, J., Choi, W. and Yoon, K., 2004. Degradation of methylene blue via photocatalysis of titanium dioxide. *Materials Chemistry and Physics*, 86(1), pp.78-82.

Liu, J. et al., 2021. Model development and performance evaluation of thermoelectric and radiative cooling module to achieve all-day power generation. *Solar Energy Materials and Solar Cells*, 220, p.110855.

Mohammed, A., Yesudasan, S. & Chacko, S., 2020. A multilayered photonic emitter for high-performance daytime radiative cooling. *Microsystem Technologies*, 27(8), pp.2873–2887.

Pourkiaei, S., Ahmadi, M., Sadeghzadeh, M., Moosavi, S., Pourfayaz, F., Chen, L., Pour Yazdi, M. and Kumar, R., 2019. Thermoelectric cooler and thermoelectric generator devices: A review of present and potential applications, modeling and materials. *Energy*, 186, p.115849.

Raman, A., Anoma, M., Zhu, L., Rephaeli, E. and Fan, S., 2014. Passive radiative cooling below ambient air temperature under direct sunlight. *Nature*, 515(7528), pp.540-544.

Speegle, W.by J. et al., 2022. Types of clouds: Discover the 4 main cloud groups. *AZ Animals*. Available at: https://a-z-animals.com/blog/types-of-clouds-discover-the-4-main-cloud-groups/ [Accessed April 22, 2022].

Sun, X. et al., 2017. Radiative Sky Cooling: Fundamental physics, materials, structures, and applications. *Nanophotonics*, 6(5), pp.997–1015.

Thermoelectric. 2022. *Power Generation - Thermoelectric*. [online] Available at: <https://thermal.ferrotec.com/technology/thermoelectric-reference-guide/thermalref13/> [Accessed 12 September 2022].

Xue, C., Wei, R., Guo, X., Liu, B., Du, M., Huang, M., Li, H. and Jia, S., 2022. Fabrication of superhydrophobic P(VDF-HFP)/SiO2 composite film for stable radiative cooling. *Composites Science and Technology*, 220, p.109279.

Yan, J., Liao, X., Yan, D. and Chen, Y., 2018. Review of Micro Thermoelectric Generator. *Journal of Microelectromechanical Systems*, 27(1), pp.1-18.

Zhao, D. et al., 2019. Radiative Sky Cooling: Fundamental Principles, materials, and applications. *Applied Physics Reviews*, 6(2), p.021306.

APPENDICES

Table A- 1: Gantt Chart for Progress Report

Project Activities	W1	W2	W3	W4	W5	W6	W7	W8	W9	W10	W11	W12	W13	W14
Understand the topic of the project and perform project planning	▓	▓												
Data gathering and literature review		▓	▓	▓	▓	▓	▓	▓	▓	▓				
Compilation of data and report writing								▓	▓	▓	▓	▓	▓	
Report writing and presentation										▓	▓	▓	▓	▓

Table A- 2: Gantt Chart for Final Year Project Report

Project Activities	W1	W2	W3	W4	W5	W6	W7	W8	W9	W10	W11	W12	W13	W14
Project planning	▓	▓	▓											
Acquiring materials needed for the project			▓	▓	▓									
Preparation of materials and sample			▓	▓	▓	▓	▓							
Setup of project						▓	▓	▓						
Data collection								▓	▓					
Report writing, poster design and presentation									▓	▓	▓	▓	▓	▓

Table B- 1: Results for Prototype A

Time	Temperature (Cold side) (°C)	Temperature (Hot side) (°C)	Temperature Difference (°C)	Voltage (mV)	Power (mW)
01:00 PM	39.8	41.1	1.3	27.6	0.3876769
02:00 PM	49.3	51.6	2.3	48.9	1.21349753
03:00 PM	49.8	50.8	1.0	21.7	0.22939462
04:00 PM	50.4	52.2	1.8	38.5	0.74323856
05:00 PM	46.6	47.9	1.3	27.5	0.3876769
06:00 PM	38.1	39.3	1.2	25.9	0.33032825
07:00 PM	33.7	34.0	0.3	6.1	0.02064552
08:00 PM	29.3	29.5	0.2	4.2	0.00917578
09:00 PM	28.1	28.7	0.6	12.6	0.08258206
10:00 PM	27.5	28.0	0.5	10.8	0.05734865
11:00 PM	28.1	28.4	0.3	6.3	0.02064552
12:00 AM	26.0	26.4	0.4	8.6	0.03670314
01:00 AM	25.4	26.0	0.6	12.7	0.08258206
02:00 AM	24.8	25.6	0.8	17.5	0.14681256
03:00 AM	25.0	25.3	0.3	6.5	0.02064552
04:00 AM	24.5	24.8	0.3	6.4	0.02064552
05:00 AM	24.6	24.8	0.2	4.1	0.00917578
06:00 AM	24.3	24.9	0.6	12.6	0.08258206
07:00 AM	24.5	25.0	0.5	10.5	0.05734865
08:00 AM	25.2	25.7	0.5	10.8	0.05734865
09:00 AM	26.2	26.5	0.3	6.3	0.02064552
10:00 AM	28.5	28.8	0.3	6.2	0.02064552
11:00 AM	31.2	31.6	0.4	8.6	0.03670314
12:00 PM	35.1	35.6	0.5	10.2	0.05734865
01:00 PM	46.5	47.7	1.2	26.1	0.33032825

Table B- 2: Results for Prototype B

Time	Temperature (Cold side) (°C)	Temperature (Hot side) (°C)	Temperature Difference (°C)	Voltage (mV)	Power (mW)
01:00 PM	39.5	41.2	1.7	35.9	0.66912392
02:00 PM	49.0	51.6	2.6	57.8	1.56514799
03:00 PM	49.5	50.9	1.4	30.1	0.45380031
04:00 PM	49.3	52.4	3.1	66.4	2.22501068
05:00 PM	46.4	48.1	1.7	36.1	0.66912392
06:00 PM	37.9	39.3	1.4	29.2	0.45380031
07:00 PM	33.6	34.0	0.4	8.9	0.03704492
08:00 PM	29.2	29.4	0.2	4.1	0.00926123
09:00 PM	28.7	28.8	0.1	2.4	0.00231531
10:00 PM	27.7	28.1	0.4	8.3	0.03704492
11:00 PM	28.3	28.5	0.2	4.0	0.00926123
12:00 AM	26.3	26.6	0.3	6.7	0.02083777
01:00 AM	25.9	26.0	0.1	2.2	0.00231531
02:00 AM	25.5	25.7	0.2	4.2	0.00926123
03:00 AM	25.2	25.5	0.3	6.5	0.02083777
04:00 AM	25.1	25.3	0.2	4.1	0.00926123
05:00 AM	24.9	25.0	0.1	2.5	0.00231531
06:00 AM	24.5	24.9	0.4	9.1	0.03704492
07:00 AM	24.8	25.1	0.3	6.1	0.02083777
08:00 AM	25.7	25.9	0.2	4.1	0.00926123
09:00 AM	26.0	26.5	0.5	10.4	0.05788269
10:00 AM	27.9	28.7	0.8	17.4	0.14817969
11:00 AM	30.8	31.8	1.0	21.2	0.23153077
12:00 PM	34.3	35.5	1.2	25.6	0.33340431
01:00 PM	46.1	47.5	1.4	29.8	0.45380031

Table B- 3: Results for Prototype C

Time	Temperature (Cold side) (°C)	Temperature (Hot side) (°C)	Temperature Difference (°C)	Voltage (mV)	Power (mW)
01:00 PM	50.6	52.5	1.9	40.3	0.83582607
02:00 PM	56.2	59.0	2.8	59.7	1.81520122
03:00 PM	47.2	50.9	3.7	79.3	3.16965622
04:00 PM	46.6	51.1	4.5	96.5	4.68849806
05:00 PM	45.3	47.1	1.8	38.4	0.75015969
06:00 PM	37.6	39.1	1.5	32.1	0.52094423
07:00 PM	31.8	33.7	1.9	40.5	0.83582607
08:00 PM	30.1	30.8	0.7	14.6	0.11345008
09:00 PM	29.2	29.8	0.6	12.6	0.08335108
10:00 PM	28.4	29.1	0.7	14.8	0.11345008
11:00 PM	27.7	28.3	0.6	12.2	0.08335108
12:00 AM	26.6	27.3	0.7	14.5	0.11345008
01:00 AM	25.9	26.9	1.0	21.7	0.23153077
02:00 AM	25.8	26.7	0.9	19.5	0.18753992
03:00 AM	25.7	26.3	0.6	12.9	0.08335108
04:00 AM	25.4	26.0	0.6	12.9	0.08335108
05:00 AM	24.7	25.8	1.1	23.6	0.28015223
06:00 AM	25.0	25.7	0.7	14.8	0.11345008
07:00 AM	24.9	25.9	1.0	21.6	0.23153077
08:00 AM	25.0	26.2	1.2	25.7	0.33340431
09:00 AM	28.4	29.5	1.1	23.4	0.28015223
10:00 AM	31.8	32.7	0.9	18.7	0.18753992
11:00 AM	33.8	34.5	0.7	14.5	0.11345008
12:00 PM	38.7	40.1	1.4	29.2	0.45380031
01:00 PM	43.9	45.6	1.7	36.8	0.66912392